3822

UNIVERSITY OF HAWAII LIBRARY

HIGH RESOLUTION MESOSCALE MODELLING OF KAUAI WINTERTIME WEATHER

A THESIS SUBMITTED TO THE GRADUATE DIVISION OF THE UNIVERSITY OF HAWAI'I IN PARTIAL FULFILLMENT OF THE REQUIREMENTS FOR THE DEGREE OF

MASTER OF SCIENCE

IN

METEOROLOGY

DECEMBER 2003

By
Christopher R. S. Chambers

Thesis Committee:

Duane E. Stevens, Chairperson
Yi-Leng Chen
Thomas A. Schroeder

Acknowledgements:

I would like to thank Duane Stevens for his help and for providing my financial support for part of this research period. I would like to especially thank Li-Yeng Chen for his help and advice, particularly on the lead up to my two required seminars. Thanks also to Tom Schroeder for his help as my third committee member. This research relied heavily on Mark Stoelinger's RIP software for producing graphical output. The use of Brandon Kern's Hydronet programs greatly eased the use of raingauge data to compare with the model. Kevin Roe of MHPCC helped me greatly in learning how to use the MM5 model, and with various computing issues. Bun Mei Takuragi saved me an eternity with his short .sun to .gif image translator program. Thanks to Tiziana Cherubini for running the kona low case. Barry Huebert and Byron Blomquist provided excellent data from the now dismantled Kokee weather station on west Kauai. Wei Wang of NCAR (aka Mesouser) provided much needed advice on MM5 issues. Thanks to Jill Nishimura and Gordon Tribble of USGS for providing the Waialeale raingauge data.

Table of contents:

1 Introduction: 1
1.1 Geography 1
1.2 Kauai weather: 3
1.3 Past Research: 7
1.4 Goals: 11
2 Setup: 13
2.1 Data input and output: 16
2.2 Domains: 17
2.3 Model Terrain: 19
2.4 Observational Data: 20
2.5 Introduction to Case Studies: 22
3 Case 1: Easterly winds of 4 to 6 December 2001 23
3.1 Background: 23
3.2 Vertical Structure: 24
3.3 Model rainfall: 28
3.4 Cross-sectional analysis: 33
3.4.1 Modeled rainfall during hours 24 to 27 (1400 to 1700 HST on 4 Dec 2001) – A modeled afternoon orographic rainfall event 34
3.4.2 Cross sections of cloud water, potential temperature and wind vectors for hours 24-27 (1400 to 1700 HST on 4 December): 35
3.4.3 Relative humidity and equivalent potential temperature hours 24 to 27: . 40
3.4.4 Trajectories hours 24-27: 45
3.5 Overall 49
4 Other Case Studies 51
4.1 Case 2: Weak southwesterly winds of 7 to 10 April 2002 51
4.1.1 Background: 51
4.1.2 Rainfall: 53
4.1.3 Surface Wind 54
4.1.4 Cross section analysis 57
4.2 Case 3: Shear line of 24 to 27 January 2000 60
4.2.1 Background 60
4.2.2 Rainfall 62
4.3 Case 4: Wintertime strong northeasterly flow of 18 to 21 January 2002 67
4.3.1 Background: 67
4.3.2 Rainfall 70
4.4 Case 5: Kona Storm of 2 to 5 November 1995 73
4.4.1 Background to case: 73
4.4.2 Rainfall 75
5 Sensitivity of rainfall to model vegetation 78
5.1 Background 78
5.2 Results 81
5.3 Discussion of vegetation sensitivity case studies: 85
6 Discussion and Conclusion: 87

6.1 Problems: 88
6.2 Discussion of key questions: 89
6.3 Future Work: 94
6.4 Conclusion: 96
7 Appendix: 99
I. THE WORLD'S WETTEST SPOT? 99
8 References: 101

Table of figures:

Figure 1-1: Kauai area map, height above sea level is in feet. 2
Figure 1-2: Mean annual rainfall Kauai (mm) from Giambelluca et al. (1986). 6
Figure 1-3: January mean rainfall (mm) 6
Figure 1-4: August mean rainfall (mm) 7
Figure 2-1: Model resolved soil type for domain 4 (1 km resolution). Light gray is clay, darker gray is sandy loam and the rest (nearly black) is water. 16
Figure 2-2: Domain set up for all cases excluding the 1995 kona low simulation. Domain dimensions and locations are given in table 1 18
Figure 2-3: Model terrain resolved in the 1 km resolution domain (domain 4). Contours are in meters. 19
Figure 2-4: Locations of the Hydronet rain gauge stations (crosses) and the Waialeale rain gauge (black dot). 21
Figure 3-1: Surface pressure analysis for the east and central subtropical Pacific for 1200 GMT on 5 December 2001 (0200 HST (Hawaiian Standard Time)). 24
Figure 3-2: Observed sounding from Lihue for 0200 HST 5 December 2001 27
Figure 3-3: Model sounding at the same location as the Lihue sounding, for 0200 HST 5 December 2001. 27
Figure 3-4: Modeled 300 hPa geopotential height for domain 1 at hour 37 (0300 HST on 5 December). Contour interval is 5 meters. Kauai is in the center of the domain. Grid marks on the side are for model grid points, so the number 10 stands for 270 km. 28
Figure 3-5: Observed rainfall at the Mount Waialeale rain gauge for the period of the Easterly wind simulation. Values represent 15 minute totals in mm. 29
Figure 3-6: 60 hour total modeled rainfall (mm) for the easterly wind simulation. Excludes the first 12 hours. The light shaded lines are isohyets plotted at 40 mm intervals starting at 10mm. The dark lines are contours for height above sea level are given for 0 meters, 500 meters, and 1000 meters. The maximum rainfall is 155 mm. The numbered dots show the rainfall observed at the Hydronet stations over the same time period. 33
Figure 3-7: Total 1 hour modeled rainfall between hour 25 and 26 (1500 to 1600 HST on 4 December 2001) in mm. 34
Figure 3-8: Same as Figure 2-3 but including lines that show where the cross sectional analyses were taken. The line oriented east to west was used for the easterly wind case. The line oriented southwest to northeast was used for the light southwesterly wind case, the shear line case, and the strong northeasterly wind case. The remaining line oriented northwest to south east was used for the 1995 kona low simulation. Cross sections were chosen to lie roughly parallel to the average surface wind direction over the period of each simulation. 35
Figure 3-9: Cloud water (shades of grey in g kg^{-1}), potential temperature (contours °K), and wind vectors (in the plane of the cross section) for hour 24 of the simulation (1400 HST 4 December 2001). A wind vector with a horizontal component long enough to reach the start of the next vector would represent a horizontal wind speed of 40 m s^{-1}. The maximum magnitude of a vertical velocity vector component is 18

Pa s^{-1} in this cross section. The maximum vector components in the horizontal and vertical are indicated in the bottom right of the figure. The cross section used here is west-east cross section across Kauai looking north. The lowland to the east is the Lihue basin. The highest point marks the Mt Waialeale region. The valley towards the west is the model resolved Waimea Canyon. 36
Figure 3-10: As Figure 3-9 except for hour 25 (1500 HST 4 December). Maximum vertical velocity component is 23 Pa s^{-1}. 37
Figure 3-11: As Figure 3-9 except for hour 26 (1600 HST 4 December). Maximum vertical velocity component is 24 Pa s^{-1} 39
Figure 3-12: As Figure 3-9 for hour 27 (1700 HST 4 December). Maximum vertical velocity component is 23 Pa s^{-1}. 39
Figure 3-13: The same cross section for hour 24 (1400 HST 4 December) as Figure 3-9 but now showing relative humidity (shades %, contours every 5%), equivalent potential temperature (white contours every 2 K), as wind vectors (in the plane of the cross section). 43
Figure 3-14: As Figure 3-13 for hour 25 (1500 HST 4 December) 44
Figure 3-15: As Figure 5-13 for hour 26 (1600 HST 4 December) 44
Figure 3-16: As Figure 3-13 for hour 27 (1700 HST 4 December) 45
Figure 3-17: Three dimensional (plotted in a 2 dimensional frame) 2 minute back trajectories shown in the same cross section as Figure 3-9. Back trajectories are interpolated from 1 hourly data and are started at different heights above the highest point in the cross section. 47
Figure 3-18: 2 minute three dimensional forward trajectories interpolated from 1 hourly data for the period between hours 25 and 26. The trajectories start from points in the cross section that are 5 km apart in the horizontal and 50 hPa apart in the vertical. 48
Figure 3-19: As figure 3-18 but for the period between hours 16 and 17 49
Figure 4-1: Surface pressure analysis for 0000 GMT 9 April (1400 HST 8 April) 52
Figure 4-2: Total modeled rainfall, excluding the first 12 hours for the weak south westerly wind case, in mm. 54
Figure 4-3: Surface wind speed (shades in m s^{-1}) and wind direction (barbs) for hour 49 (1500 HST 8 April 2002). 56
Figure 4-4: As Figure 4-3 but for hour 61 (0300 HST 9 April 2002) 57
Figure 4-5: Cloud water (shades of grey in g kg^{-1}), potential temperature (contours in K) and wind vectors for the southwest northeast oriented cross section shown on Figure 3-8. The maximum vector in the horizontal is 13.9 m s^{-1} (if a horizontal vector component were to reach the beginning of the next then the horizontal wind speed would be 40 m s^{-1}) and in the vertical is 8 Pa s^{-1}) Plotted at hour 49 of the simulation (1500 HST on 8 April 2002), the same time as the surface wind plot of Figure 4-3.58
Figure 4-6: As Figure 4-5 but for hour 61 (0300 HST 9 April), the same time as the surface wind plot of Figure 4-4. Maximum vertical velocity vector is 12 Pa s^{-1}. ... 59
Figure 4-7: Surface pressure analysis for 1200 GMT January 26 (0200 HST, 26 January 2000). 61
Figure 4-8: Model geopotential height at 300 hPa for domain 1 at 1500 HST on 26 January, contour interval is 5 meters 62
Figure 4-9: Total modeled rainfall in mm, excluding the first 12 hours, for the shear line simulation 63

Figure 4-10: South west to north east oriented cross section (as in Figure 4-5) showing relative humidity (colors, %), equivalent potential temperature (white contours in K) and wind vectors for hour 40 (0000 HST 26 January 2000). Maximum vertical velocity vector magnitude is 30 Pa s^{-1} (this occurs in the down-slope flow just to the lee of W). 66
Figure 4-11: Surface pressure analysis for 1200 GMT (0200 HST) 19 January 2002.... 67
Figure 4-12 Wind speeds (shades m s^{-1}) and directions (barbs: one full barb is 5 m s^{-1}) at 400 hPa for hour 36 (0200 HST 19 January 2002) 68
Figure 4-13: Total 60 hour rainfall (mm) excluding the first 12 hours of the strong northeasterly wind case. 70
Figure 4-14: Relative humidity (colors in %) theta-e (contours in K) and wind vectors (arrows) for a SW to NW cross section across Kauai for hour 36 (0200 HST 19 January 2002) of the strong northeasterly wind simulation. This cross section is thicker (1000 hPa – 300 hPa) than those of the previously discussed simulations. Maximum vertical velocity vector component is 21 Pa s^{-1}. 72
Figure 4-15: Modeled geopotential height (m) at 300 hPa for 0200 HST 3 November 1995. Contours are every 5 m. 74
Figure 4-16: 60 hour total rainfall (mm), excluding the first 12 hours of the simulation, for the 1995 kona low case. 75
Figure 5-1: Total 60 hour rainfall for the easterly trade wind case for a) evergreen broadleaf forest b) mixed forest and c) sparse vegetation. 83
Figure 5-2: 60 hour total rainfall for the strong northeasterly wind case for a) mixed forest and b) sparse vegetation. 84

Abstract:

Across the island of Kauai there are enormous gradients of rainfall, and in the center of the island Mt Waialeale is considered one of the wettest spots on Earth. Five high resolution MM5 case studies under different wintertime synoptic flow regimes have been performed to investigate the processes that lead to the observed rainfall distributions across the island. There is good agreement between the modeled rainfall and 3 day rain gauge totals for 4 out of the 5 case studies presented. This suggests that rainfall distributions and gradients across the island are to some extent realistically simulated. Analysis of the easterly wind case reveals significant structural changes to the trade wind layer as it passes over the island. On approach to the central mountains, there is a general deepening of the moist layer and a corresponding deepening of clouds associated with flow over, rather than around, the island. On the lee side downward moving air mixes dry air from above the inversion with the moist air below, leading to a drying of the moist layer over leeward areas. Trajectory analysis suggests that, aided by latent heat release, air from low levels under partially cloudy (i.e. trade cumulus) easterly wind conditions can lift up the windward slopes and flow over the top of Waialeale. Persistent heavy rainfall out of the consequent deep orographic clouds is triggered as upward motion shifts to downward motion over the summit. Wind flow changes over the summit crest are in turn likely to be largely dependent on the characteristics of the trade wind inversion.

Other case studies under different synoptic flow also produce a maximum in rainfall over Waialeale. Results suggest, but do not prove, general intuitions about the conditions that favor the production of orographic rain. A deeper moist layer allows the

development of deeper clouds leading to greater rainfall. Latent heat aided uplift within orographic clouds supports the flow of air over the mountains.

Model testing of sensitivity to vegetation specification reveals that changing the vegetation type in the model leads to different total rainfall patterns across the island. These differences result as (either) a local island consequence of the altered surface fluxes associated with the vegetation changes made, and (or) the simulations producing different cloud and rain distributions generated by a separate forecast.

1 Introduction:

1.1 Geography

Kauai is the northernmost of the main Hawaiian Islands centered at 159°30'W, 22°5'N. The island is a 5 million year old extinct volcano. As a consequence of its age Kauai is a heavily eroded island with deep valleys and steep cliffs. Figure 1-1 shows the shape and topography of the island. It is up to 49 km (30 miles) long (east-west orientation) and up to 40 km (25 miles) wide (north-south). The island has a land surface area of 1,430.5 square kilometers (552.3 square miles). The northwest facing shore named the Na Pali coast consists of a dramatic combination of steep cliffs and steep valleys leading up to the 900-1300 meter high mountains a few kilometers inland. The north coast becomes less mountainous toward the east, leading to the mostly flat or gently sloping Lihue Basin that dominates the east of the Island. The south and southwest coast is the driest area of the island. Inland from the southwest coast deep canyons have eroded into the extinct volcano, most notably the 500-1000 meter deep Waimea Canyon. Approximately in the center of the island are the two highest points of the island, Mt Kawaikini (1598 m) and 2 km to the north Mt Waialeale (1569 m). The Mt Waialeale rain gauge is located on the ridge between these two summits. Plummeting down to the east of these peaks is Waialeale crater, a spectacular cirque of cliffs that are over 1000 m high and striped with waterfalls (dependent on rain). Significantly, these cliffs face the Lihue Basin to the east; therefore no major mountains lie to the east of the two highest points and the rain gauge. To the west of the summit ridge lies the Alakai Swamp, a

large plateau swamp that covers the gently sloping areas between 1300 m to 1500 m and ends near the top of the Waimea Canyon.

The island is heavily vegetated, hence its nickname The Garden Isle. As well as the high plateau swamp, the interior is dominated by wet forest and woodland, particularly over the northern areas of the island. Areas of the lower, flatter elevations, mainly over eastern areas, have been altered by human activity into arable (e.g. sugar cane, taro) and small urban areas (e.g. Lihue, the largest town on the island, population = 5536 in 1990).

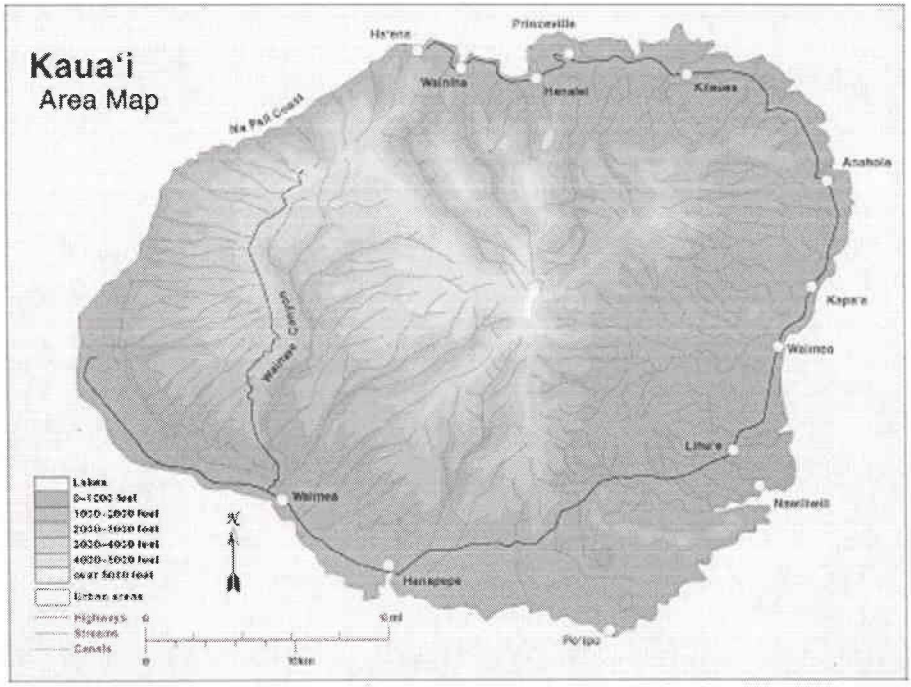

Figure 1-1: Kauai area map, height above sea level is in feet.

1.2 Kauai weather:

The enhancement of rain, compared to the open ocean value, over Kauai per unit area is the greatest of all the Hawaiian Islands at 3.4 times the open ocean value (Nullet and Mcgranghan 1988). The next wettest island per unit area is Maui with 2.8 times the open ocean value. Rain gauge observations have shown that annual rainfall is greatest within the interior of the island and least along the southwest facing coast (Fig. 1-2). At the Waialeale rain gauge, in excess of 11,000 mm of rain falls annually; a discussion as to whether this is the wettest spot on Earth is provided in appendix I. 15 km away from Waialeale, the southwest coastal regions of the island receive less than 750 mm of annual rainfall. The East coast receives between 1000 mm and 1500 mm annually and the north coast between 1500 mm and 2500 mm.

The available rainfall data from central Kauai suggests that there may be some extremely large annual rainfall gradients near the summit of Waialeale. Figure 1-2 suggests that to the east of the summit rainfall maximum, the gradient in annual rainfall may be around 2100 mm km^{-1} yr^{-1}. This depends on the accuracy of the annual rainfall map, which depends on the spatial availability and accuracy of the rain gauge data in this area and how that data is analyzed. Clearly there are extremely large gradients in average annual rainfall in this region, possibly some of the largest in the world.

The climate of the Hawaiian islands is dominated by the northeasterly trade winds that prevail 85 to 95 % of the time in summer and 50 to 80 % of the time in the winter (Sanderson 1993). The trade wind vertical structure consists of a shallow moist layer capped by a trade wind inversion (TWI) at a mean height of 2000 m (Sanderson 1993) that usually lies above the highest mountains on Kauai. The persistent summer trade

winds can get disrupted by the passage of tropical systems, usually in the depression or disturbance stage but occasionally as a tropical storm or hurricane. The most notable event being Hurricane Iniki that devastated Kauai on 11 September 1992 bringing winds of 130 mph and costing between $2 to $3 billion (Sanderson 1993). Upper-tropospheric disturbances above the lower troposphere trade wind flow can lift or remove the TWI, sometimes enabling deep convection and heavy rain at any time of the year. The winter time trade winds are frequently disrupted by the passage of cold fronts that have penetrated into the subtropics. These are often slow moving and decaying and are called shear lines because of their more characteristic wind shear rather than a large temperature gradient. Kona lows (upper level extra-tropical lows that show a surface signature) occur mainly between October and March and can bring heavy rain, strong winds and high surf especially to the usually dry leeward areas of the islands. Kauai, being the furthest north of the main Hawaiian islands receives the most winter storm and frontal activity (Sanderson 1993)

The distribution of rainfall across the island varies somewhat throughout the year. January and August average rainfall distributions shown in Figures 1-3 and 1-4 show this seasonal variation in rainfall. Monthly average rainfall at the Waialeale rain gauge varies between 700 mm in June, September and October to 1100 mm in December. Even though monthly rainfall is highest over the winter months, significant rain occurs in every month of the entire year. Seasonal variations are more marked over the leeward lowland stations. Kekaha on the southwest coast receives an average of 98 mm of rain in December but only 11 mm in June. This large annual variation in Kauai leeward rainfall is consistent with other rainfall stations that lie on the lee side of the other Hawaiian

Islands (with the notable exception of some of the Big Island stations that lie in the lee of Mauna Kea and Mauna Loa which have a rainfall peak in summer, this is likely related to the dependence of rain on afternoon convective rainfall, caused by island heating and enabled by the sheltering effect of the massive volcanoes during dominant trade wind conditions during summer). The wintertime rainfall maximum over leeward areas is due largely to widespread rainfall from synoptic systems such as cold fronts and Kona Storms that pass over the islands during the winter months. The seasonal variation in rainfall is less over windward and mountainous areas of Kauai because these areas receive summer trade wind rainfall of a comparable amount to wintertime rainfall (largely trade wind rainfall as well). Trade wind rainfall is strongly related to orography and consequently there are larger rainfall gradients across the island during the summertime when trade winds dominate. Rainfall information for this paragraph has been interpreted from Giambelluca et al. (1986).

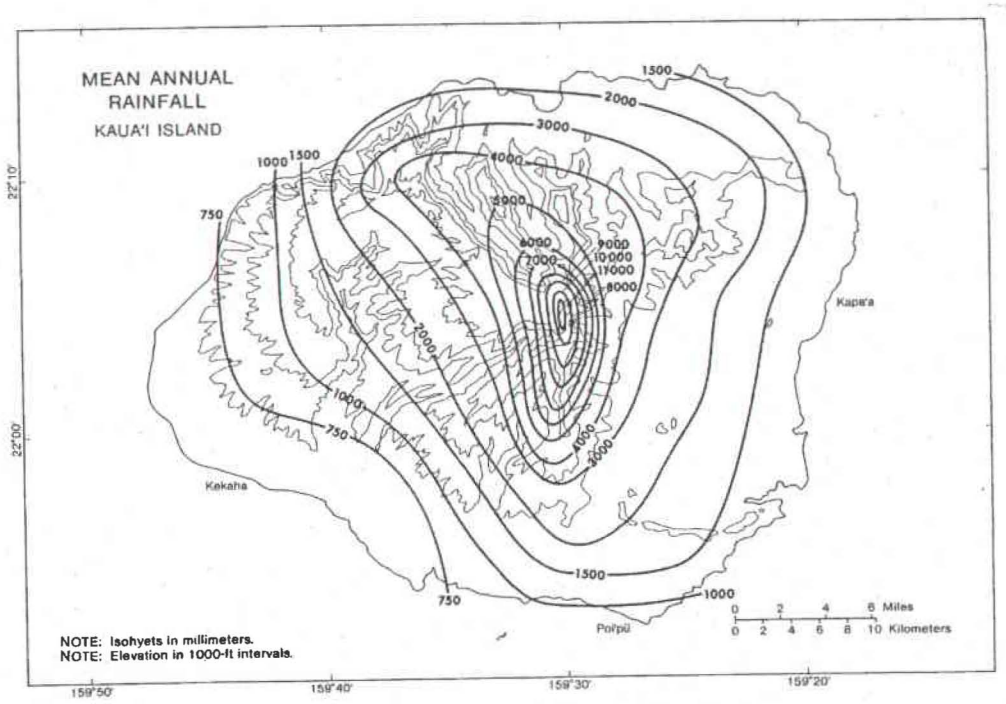

Appendix Figure A.118. Mean annual rainfall, Kaua'i Island, Hawai'i

Figure 1-2: Mean annual rainfall Kauai (mm) from Giambelluca et al. (1986).

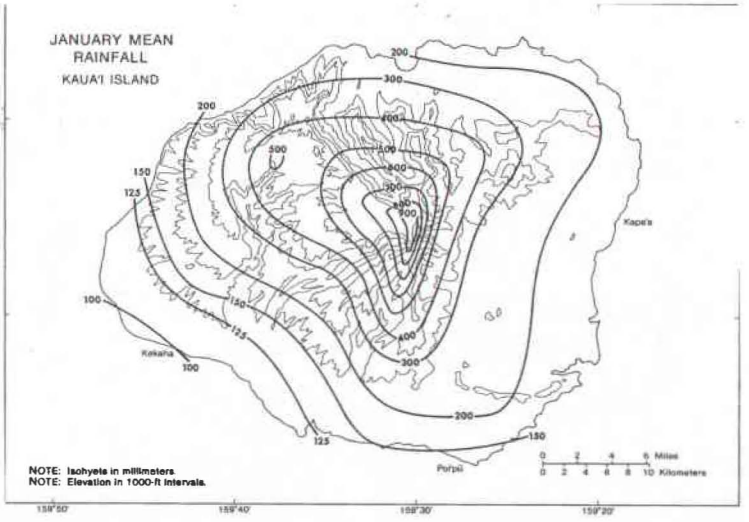

Appendix Figure A.119. January mean rainfall, Kaua'i Island, Hawai'i

Figure 1-3: January mean rainfall (mm)

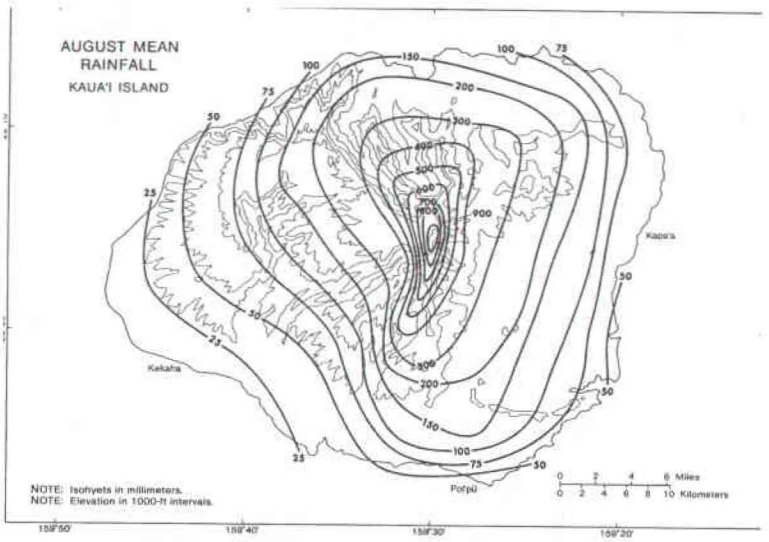

Appendix Figure A.126. August mean rainfall, Kaua'i Island, Hawai'i

Figure 1-4: August mean rainfall (mm)

1.3 Past Research:

Leopold (1949) explained the low level wind flow over the Hawaiian Islands as a combination of the large scale trade wind flow interacting with the island topography and the locally generated thermal flow (sea/land breezes). For the smaller islands with lower mountains he stated that flow is over the top rather than around the side of the mountains (as is the case for the Big Island and east Maui). Cloud lines associated with sea breeze and trade wind convergence were thought to produce significant rainfall and affect the microclimates of the islands.

Lavoie (1974) used a very simple one layer model to study trade wind interactions with the island of Oahu. The model simulated a lifting of the inversion top upwind of the Koolau Mountain Range (KMR) by about 200 m under the modeled trade wind conditions. A rapid lowering of the inversion top occurred over the crest of the KMR but

there was sharp rise in the inversion over leeward areas. This sharp dip and rise in the inversion was stated as a consequence of a mild hydraulic jump in the lee of the KMR. A marked drying in the trade wind layer humidity occurred between the windward and leeward shores. He suggested that this was a combination of removal of moisture through rainfall and mixing of dry air from aloft with moist air below. A simulation with no rainfall still produced lee drying adding weight to the argument that dry air mixing from aloft plays an important role in leeside drying. Leeside drying led to a lifting of the lifting condensation level and to shallower clouds over lee areas. This was suggested as being the reason why the Waianae Range received much less rainfall than the KMR in this study.

Woodcock (1975) looked at rainfall observations from anomalous orographic rain (AOR) events over the KMR of Oahu. Rainfall at stations leeward but near the KMR crest was observed to be 15 times greater than that observed at the windward coast. This suggested that a very rapid rainfall generation process was occurring between the coast and the mountains. Woodcock suggested that this may be occurring due to enhanced small droplet growth due to wind shear and turbulence induced by the island topography, combined with the input of moist air by the island.

Takahashi (1981) analyzed aircraft observations of trade wind clouds off the coast of windward Hawaii (the Big Island). He observed that a convergence region where the trade winds met air flowing offshore led to a lowering of the cloud base. This lowering of cloud base enabled the formation of larger cloud droplets to form in the deeper cloud. He also observed that cloud droplets grow large during horizontal traverses through clouds developing along the direction of the prevailing wind. The deceleration of the

updraft in the vertical near the cloud top was thought to be a crucial factor in enabling rapid growth of drizzle droplets. Droplets of a certain size would fall until they met a strong enough updraft to push them back up enabling further growth. This would continue until the drop was heavy enough to fall against the updraft or if it entered a region with weaker updrafts or downdrafts. A droplet peak size then increases by around 20% as it falls to the cloud base.

Durran (1986) in a simulation sensitivity case study of a Boulder (Colorado) windstorm, found that the presence of a low level inversion above the mountain top was essential in reproducing the windstorm. The thickness of the fluid (between mountain top and inversion) decreases as air ascends the mountain range. If there is sufficient increase in velocity and decrease in thickness, a transition from sub critical to supercritical flow occurs at the summit crest. Supercritical flow down lee slopes continues to accelerate until eventually recovering to the ambient downstream conditions in a turbulent hydraulic jump. Given the findings of Durran's study, the trade wind inversion is likely to play an important role in the production of down-slope winds on the Hawaiian Islands.

Smorlarkiewicz and Rotunno (1989) looked at density stratified fluid flow past a 3D obstacle. In their experiments the transition from Fr = 0.66 to Fr = 0.22 (Fr = U/Nh where U is the wind speed, N is the buoyancy frequency, and h is the height of the mountain obstacle) produced a dramatic change in the flow regime near the obstacle. At Fr = 0.66 windward uplift and leeside down slope flows were stronger than at Fr = 0.22. As the Fr decreased lateral deflection of the flow increased leading to the generation of leeside vortices. Model results confirm observational evidence that lee island vortices

around the Big Island are more prevalent than on the other, smaller and lower Hawaiian Islands.

Taking typical trade wind conditions of $N = 0.01\ s^{-1}$, and $U = 10\ m\ s^{-1}$ and for the Big Island a mountain height of 4100 m, gives a Froude number of $Fr = 0.24$. A mountain height of 1500 m, close to the height of Mt Waialeale, leads to a Froude number of $Fr = 0.66$. For this lower mountain height Smorlarkiewicz and Rotunno's simulations suggested that Kauai would have less lateral deflection of the flow and greater orographic uplift (associated with greater air flow over the island) than the Big Island.

Ramage and Schroeder (1999) looked at observed trade wind rainfall from Mt Waialeale. Raindrops over Waialeale are rarely more than 2 mm in diameter; however daily totals exceeding 50 mm are not uncommon. They found that significant rain only occurs when an area of cloud extends upwind. Trade wind strength was found to be positively linked to Waialeale rainfall but not with Lihue rainfall, suggesting that orographic uplift did not extend to the coast. Moist layer depth was also found to be positively correlated with Waialeale rainfall as a deeper moist layer is able to support deeper clouds and therefore generally produces greater rainfall. Rainfall at Waialeale was found to vary diurnally with a predawn maximum and an afternoon minimum. This diurnal variation was said to be related to increased cloudiness in the early morning hours over the open ocean due to nocturnal radiational cooling of the top of the moist layer.

Chen and Feng (2001) performed modeling simulation sensitivity case studies for the Big Island of Hawaii. They showed that the height of the trade wind inversion affects the depth and locations of the clouds over the Big Island. Deeper more extensive clouds

extend further inland and upslope when there was a high inversion. They also found that the low inversion case showed greater deflection of the flow around the island than the high case. Diabatic heating was shown to enhance vertical motions in cloudy areas over the windward side of the Big Island and to weaken island blocking.

1.4 Goals:

I use the Pennsylvania State University-National Center for Atmospheric Research (NCAR) nonhydrostatic mesoscale model version five (MM5) to investigate the production of rainfall over the island of Kauai. The approach is to use 3 day high resolution simulations of different real weather cases. This approach has its advantages and its disadvantages. Using real cases means that the model is attempting to recreate a real atmospheric situation. We are therefore able to compare with observations over the time period considered and assess, to some degree, the accuracy of the model. Disadvantages arise mainly in interpretation and analysis of the data. Real cases evolve in the changing synoptic environment. Therefore difficulties arise when establishing the specific causation of features that evolve in time, for example diurnal circulations.

Specific goals of this study include:

1.) To perform high resolution 3 day MM5 simulations focusing on the Island of Kauai for 5 different wintertime large-scale synoptic flow regimes.

2.) To establish how well the model simulates rainfall distributions across the island for these cases.

3.) To investigate the structure of the lower troposphere over Kauai under these different synoptic regimes.

4.) To investigate in relation to previous studies the primary mechanisms responsible for producing the high rainfall gradients across the island.

5.) To discuss the results of these simulations in reference to the question: Why is Mount Waialeale one of the wettest spots on Earth?

2 Setup:

The case studies presented here were run on the 5th generation National Centers for Atmospheric Research (NCAR)/Penn State mesoscale model (MM5). MM5 is the latest incarnation of an evolving model that was first created in the early 70s. The model was initially hydrostatic and was presented by Anthes and Warner (1978). The model has since undergone a number of changes including becoming non-hydrostatic (Dudhia 1993). The hydrostatic approximation effectively limited the horizontal resolution to 10 km. The non-hydrostatic version has enabled higher resolutions and smaller scales to be studied.

The model has a multiple nesting capability enabling studies of specific areas at high resolutions. Multiple nesting is particularly useful for Hawaii because of the need to accurately represent complex topography over a small area while at the same time modeling synoptic scale features.

The MM5 allows the user to choose from an assortment of different available schemes that represent the physics of the modeling system. These schemes include (i) cumulus parameterization (ii) planetary boundary layer (iii) explicit moisture, and (iv) radiation. For consistency the same model physics setup was used for all the cases in this study. The setup used here is similar to that used by Chen et al. (2001) who studied a heavy convective rainfall event in Colorado down to 1 km horizontal resolution.

The planetary boundary layer is parameterized using the Medium-Range Forecast (MRF) model of NCEP. This scheme is based on Hong and Pan (1996) and is the most popular PBL scheme in MM5 for multiple nested studies. As emphasized in Hong and

Pan (1996) the formulation of the PBL scheme is of comparable importance to accurate precipitation forecasts as the cumulus parameterization scheme.

The Grell cumulus parameterization scheme of Grell (1993) is used on the 27 km and 9 km resolution domains. On the advice of Jimy Dudhia of NCAR, no cumulus scheme was used on the 3 km and 1 km resolution domains. On the 3 km and 1 km resolution domains, cloud and moist processes are therefore solely represented by the explicit microphysics scheme.

The Reisner Mixed-Phase explicit moisture scheme is used on all domains. For details refer to Reisner et al. (1998). This scheme considers super cooled water as well as allowing for the slow melting of snow. Memory is added for cloud ice and snow, though no graupel and riming processes are considered. Kauai rainfall is predominantly formed through warm rain processes because trade wind clouds usually lie below the freezing level. Only the deeper convection, associated with the Kona low case in particular, will be using the ice phase processes within the clouds that are producing precipitation. The Reisner microphysics scheme parameterizes the following warm rain processes:

1) Conversion from cloud water into rain water: The Kessler parameterization scheme is used to parameterize the collision and coalescence of cloud droplets.
2) Collection of cloud water by rain water.
3) Sublimation/evaporation of rain water
4) Conversion from water vapor into cloud water

Further details can be found in the appendix of Reisner (1997).

The atmospheric radiation balance is computed using the cloud-radiation scheme. This scheme considers long wave and shortwave interactions with explicit cloud, clear air and precipitation. This scheme provides surface radiation fluxes as well as atmospheric temperature tendencies.

The Land Surface Model used in these simulations is discussed in Chen et al. (2001). This model has one canopy layer as well as 4 soil layers at depths of 0.1, 0.3, 0.6, and 1.0 m. For each of the soil layers the volumetric soil moisture and temperature are calculated. For the canopy layer the water stored is calculated. The root zone is in the upper 1m of soil and below 1 meter there is gravity drainage of water.

The LSM is limited by the data available for defining the soil type and vegetation type over a specific area. As this project has progressed the standard vegetation data for MM5 over the Hawaiian islands has changed from being totally homogenous savanna, to being almost totally mixed forest. The only exception to mixed forest occurs over Honolulu where there is an area of urban land in the Honolulu region. Therefore for the island of Kauai the vegetation is defined as mixed forest over the whole island. The reality is quite different from this, with a variety of vegetation across the island ranging from agricultural (sugar cane, taro) mainly over east Kauai, tropical rainforest on windward slopes and in the mountain valleys, swampland in the elevated interior plateau (Alakai Swamp), and drier scrubland in leeward areas.

The model has only two soil types for Kauai. These are sandy loam and clay. The distribution of the different soils is shown in Figure 2-1. This is not a realistic distribution of soil types and is a serious deficiency for the accurate modeling of island thermal circulations.

Figure 2-1: Model resolved soil type for domain 4 (1 km resolution). Light gray is clay, darker gray is sandy loam and the rest (nearly black) is water.

2.1 Data input and output:

With the exception of the 1995 kona low case study, all of the simulations were initialized using NCEP Global Tropospheric Analyses (known as the ds083.2). The analyses are from the NCEP Final Analyses (FNL) which is currently the same as the Aviation (AVN) run except that a later input data cutoff time is used. This GRIB formatted dataset is available at 6 hourly intervals at times 0000 GMT, 0600 GMT, 1200 GMT, and 1800 GMT daily. It has 24 levels in the vertical and a resolution of 1 x 1 degree (latitude, longitude) in the horizontal. As well as atmospheric data, this dataset contains the variables skin temperature, water content of soil, soil temperature, and sea surface temperature. This data set has been archived since September 1999. For the 1995 kona low case study, the coarser 2.5 x 2.5 degree resolution dataset was used.

For all simulations model data was output every hour. The data was analyzed using two software packages: 1) Read Interpolate Plot (RIP) and 2) Graph (NCAR graphics package).

2.2 Domains:

4 domains are used for all the cases in this study. The domain setup is shown in Figure 2-2. Domains 1, 2, 3 and 4 have resolutions of 27 km, 9 km, 3 km, and 1 km respectively and the dimensions are shown in Table 1. The only exception to this setup is the 1995 Kona low simulation. This simulation had the same number of domains and resolutions but the outer domain was much larger with the number of x, y grid points being 151,133. This larger outer domain was set up so that the entire evolution of the kona low would fit within it.

Domain number	Resolution (km)	Number of grid points (x,y)	Size of domain (x,y (km))	Position of domain
1	27	61, 61	1647,1647	Centered on 22.1°N, 159.50°W
2	9	55, 52	495,468	Southwest corner point at point 22,22 of domain 1
3	3	58, 40	174,120	Southwest corner point at point 16, 21 of domain 2
4	1	82, 67	82,67	Southwest corner point at point 22,10 of domain 3

Table 1: Domain dimensions for all cases except for the 1995 kona low simulation

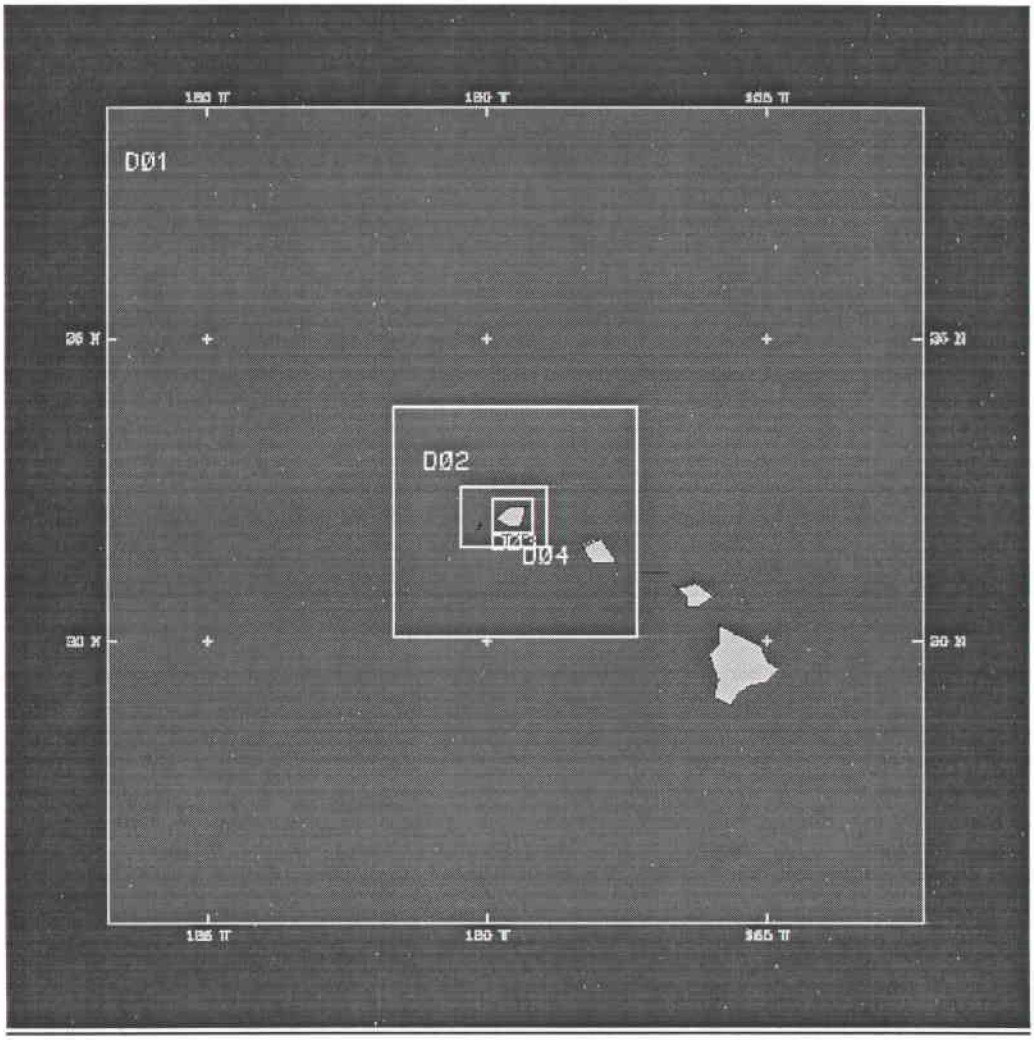

Figure 2-2: Domain set up for all cases excluding the 1995 kona low simulation. Domain dimensions and locations are given in table 1

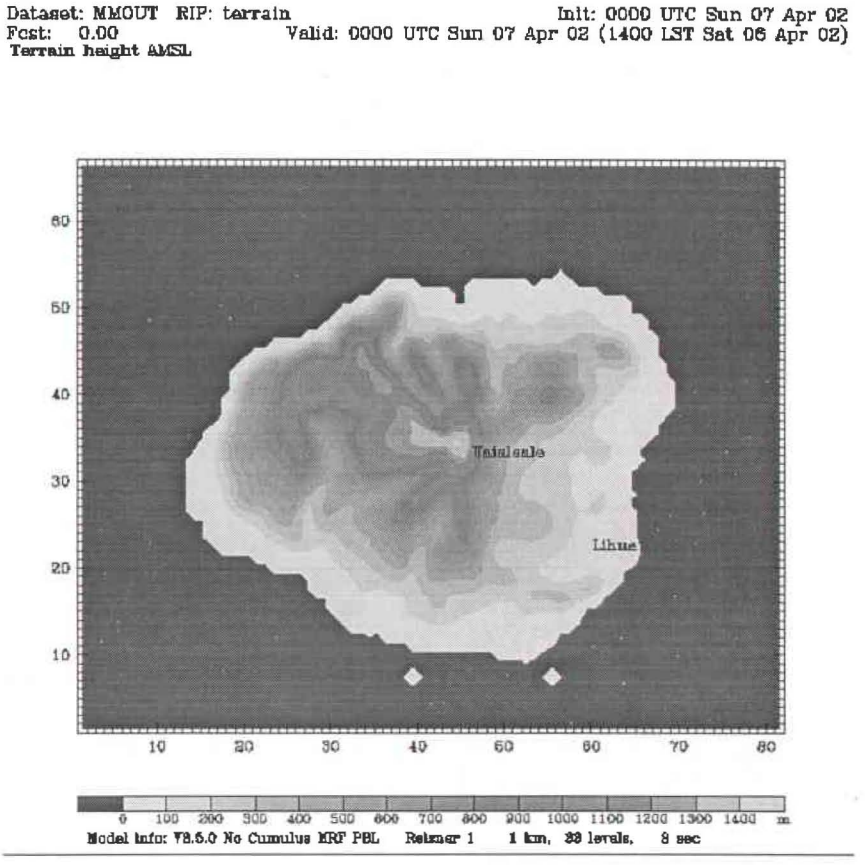

Figure 2-3: Model terrain resolved in the 1 km resolution domain (domain 4). Contours are in meters.

2.3 Model Terrain:

The model orography for domain 4 (1 km resolution) is shown in Figure 2-3. At this resolution the model manages to capture a lot of the orographic features of the island shown on Figure 1-1.

The highest point in the model is 1422 m compared to the 1598 m elevation of the actual highest point (Kawaikini) and 1569 m of Mt Waialeale. The model therefore shaves 176 m off the highest point due to the 1 km resolution smoothing. Smoothing also produces one model peak near Mt Waialeale and this highest point is also displaced slightly to the west. In a region with large rainfall gradients over small distances these

differences need to be appreciated when interpreting the model results. The highest point resolved in the model will be called W in the following chapters.

The modeled terrain reproduces smoothed versions of the main valleys on the island. The Waimea Canyon in west central Kauai can be seen in the model terrain as the westernmost main valley. The smoothing of the terrain leads to these valleys being shallower than reality. This means that the base of Waimea Canyon in the model is significantly higher than the observed Canyon floor. Also at this resolution the model cannot capture the many smaller valleys that occur in the mountains. Because of this the actual total surface area of the island may be significantly larger than the modeled surface area. At smaller scales still the steeper mountains and cliffs of the island are characterized by fluting. These and other small scale erosional features may have important effects on near surface turbulence and surface fluxes around the island. In particular the Na Pali (northwest Kauai) coast has a much larger surface area than the smoothed model terrain in this region. It can be imagined that if these coastal mountains and valleys were stretched out like an accordion they would cover a much larger surface area than the model has. The conclusion can only be that the modeled land surface is highly inaccurate in these regions (and others probably). The correct modeling of island thermal circulations may be particularly sensitive to surface fluxes and so may suffer as a result of a smoothed island in the model.

2.4 Observational Data:

Rainfall data was available through the Hydronet system for all the case studies. Hydronet provides 15 minute rainfall data and so provides detailed rainfall data

for each station. The locations of the Hydronet stations are shown in Figure 2-4. Comparing Figure 2-4 and Figure 1-2 we can see that the available stations are mostly nearer the coasts of the island away from the exceptionally wet interior.

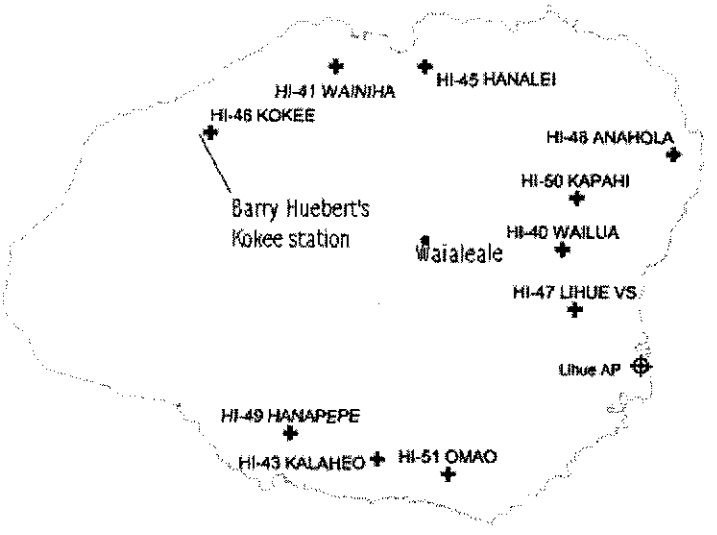

Figure 2-4: Locations of the Hydronet rain gauge stations (crosses) and the Waialeale rain gauge (black dot).

The Waialeale rain gauge lies on the ridge between Mt Kawaikini and Mt Waialeale. Because of the remote location of this rain gauge, it is automated and is checked by helicopter approximately once a month depending on weather conditions. These difficulties lead to a discontinuous record however data was available throughout the simulation periods of this study and so it was used. The rainfall is recorded every hour.

In addition to this data a weather station at Kokee, west Kauai was used primarily to set up the cases (Barry Huebert personal communication).

2.5 Introduction to Case Studies:

The simulations performed in the order that they will be discussed in the following sections are:

1) 0000 GMT, 4 to 0000 GMT, 6 December 2001: Easterly wind case.
2) 0000 GMT, 7 April, 2002 to 0000 GMT, 10 April, 2002: Light Southwesterly winds.
3) 1800 GMT, 24 January, 2000 to 1200 GMT, 27 January, 2000: Shear line case.
4) 0000 GMT, 18 January, 2002 to 0000 GMT, 21 January, 2002: Strong northeasterly winds.
5) 1200 GMT, 2 November, 1995 to 1200 GMT, 5 November, 1995: Kona Storm (Businger et al. 1998)

Case 5 has the following differences from the other cases: 1) Domain 1 is substantially larger so that the Kona Storm evolves largely within the outer domain. 2) Although the simulation had 33 layers, the layers were at different levels. 3) The simulation did not use the Land Surface Model. 4) As mentioned in section 2.1 coarser resolution (2.5 by 2.5 degree) initial data was used

W will refer to the highest point on the island as resolved by the model. As discussed earlier the elevation of W is 1422 m above sea level. This is considered to be the location on the model terrain that corresponds best to the location of the rain gauge in reality.

3 Case 1: Easterly winds of 4 to 6 December 2001

3.1 Background:

This research will focus mainly on this simulation as it represents the closest to typical trade wind conditions of the 5 case studies performed. A high pressure system lay to the northeast of the islands throughout this period. The center of the high lay at 145°W, 37°N at the start of the simulation (0000 GMT on 4 December 2001) with a central pressure of 1036 hPa. The high migrated slightly southeastwards during the first 12 hours before becoming near-stationary around 140°W, 35°N for the remainder of the simulation. The surface pressure for 1200 GMT on December 5th is shown on Figure 3-1. The central pressure remained between 1030 hPa and 1035 hPa throughout. Throughout the 72 hours of the simulation easterly surface winds were blowing across the Hawaiian Islands. An approximate open ocean wind speed of 10 m s^{-1} corresponds to Fr = 0.66 (assuming N = 0.01 s^{-1} for consistency with Smorlarkiewicz et al. (1988) and Chen and Feng (2001), and h = 1500m).

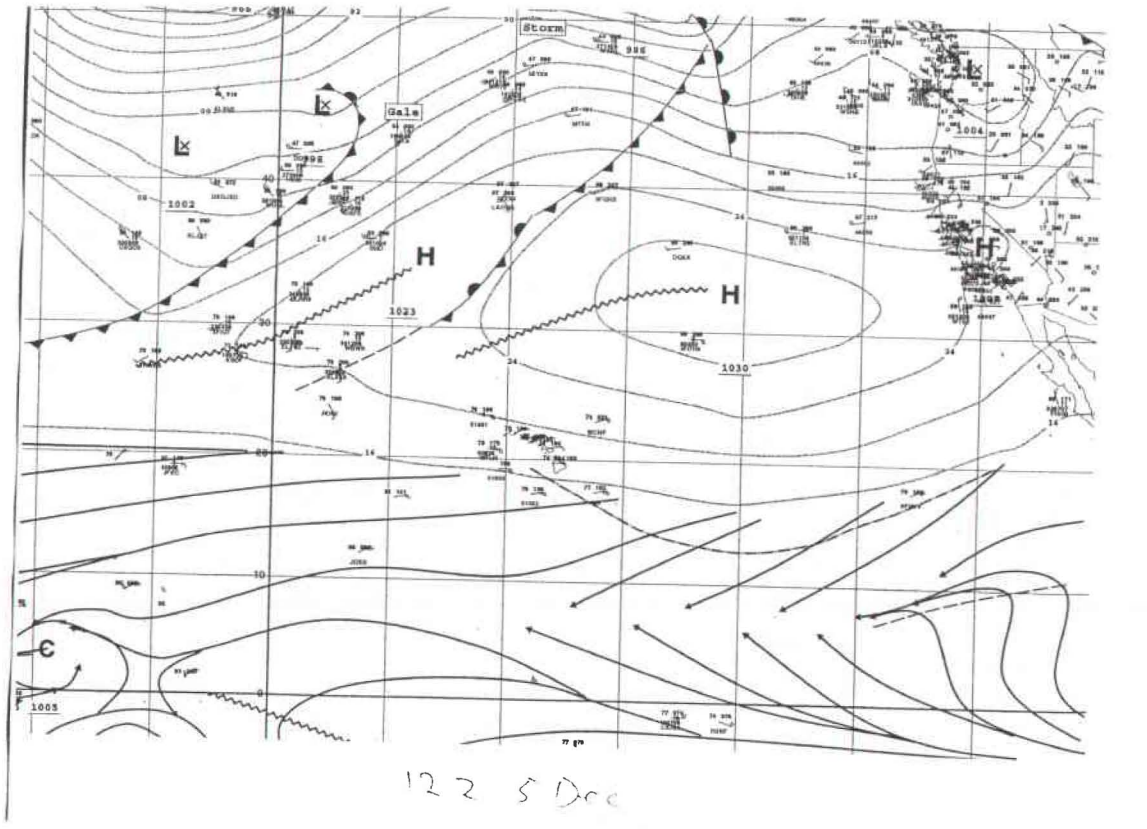

Figure 3-1: Surface pressure analysis for the east and central subtropical Pacific for 1200 GMT on 5 December 2001 (0200 HST (Hawaiian Standard Time)).

3.2 Vertical Structure:

An important question that needs to be addressed is: How well does the model simulate the vertical structure of the atmosphere over Kauai? Kauai is one of the two islands where a rawinsonde is launched regularly. This launch occurs every 12 hours from Lihue near the east coast. At the same location and at the same times of the Lihue launch, for this case, a sounding was plotted using the model output data. An example of the observed sounding from 1200 GMT on 5 December (0200 Hawaii State Time (HST),

hour 36 of the simulation) is shown on Figure 3-2. Figure 3-3 shows the model sounding for the same time and location.

In general the model and the observed sounding qualitatively agree on the vertical structure of the atmosphere above Lihue. Both the model and the observed sounding show the trade wind inversion (TWI). The TWI base was about 20 to 50 hPa lower in the model than in the observed during the first 24 hours of the simulation, at around 720 hPa in the model. There was good agreement in the TWI height around 800 hPa for the remainder of the simulation apart from the final hour (1200 GMT 7 December) when the model kept the inversion base at 800 hPa whereas the observed sounding had it at 750 hPa. It should be noted here that the 2 soundings are probably over increasingly different regions, at higher altitudes because the balloon of the observed sounding will have traveled a distance from its original location in the horizontal as it is blown by the winds. For example a balloon blown at 10 m s^{-1} for 30 minutes would have traveled 18 km in the horizontal and could lie over the inland mountains. The model sounding simply represents the direct vertical profile above Lihue.

I have looked at 6 hourly soundings to provide an overview of the vertical profiles of this simulation. A conditionally unstable layer existed within the trade wind moist layer up to the TWI. The sounding was generally dry-adiabatic up to the LCL that lay between 900 and 950 hPa. The stable TWI was present throughout the simulation inhibiting the development of deep clouds with the inversion base at between 800 hPa and 700 hPa. Above the inversion air was conditionally unstable to heights of around 400 hPa although the lapse rates within this layer were nearly moist-adiabatic. Convective available potential energy (CAPE) was usually near zero but was largest in

hour 24 when it was 227 J kg^{-1}. When compared to the observed Lihue sounding the model tended to underestimate CAPE. For example at hour 24 (1400 HST on 4 December) the observed CAPE was 586 J kg^{-1}, however both the model and the observations agree on this time as having the maximum CAPE over the period analyzed. The K index average of 7 corresponds to a 0 % probability of thunderstorms. The low K index is typical of trade wind conditions because of the stable trade wind inversion below 700 hPa and the very dry air above it. The K index increases when the lapse rate is unstable with abundant low-level moisture extending to at least 700 hPa and is defined in George (1960) as:

$$K = (T_{850} - T_{500}) + T_{d850} - (T_{700} - T_{d700})$$

Where suffixes of numbers represent pressure levels in hPa and T_d represents the dew point temperature.

Over the simulation period an ascending directional shift in wind from south-easterly to westerly occurred between 400 and 600 hPa. Both the model and observations agreed on the presence of generally strong westerly winds around 300 hPa. Geopotential height at 300 hPa shown on Figure 3-4 shows that the westerly winds at this height were associated with large scale westerly flow.

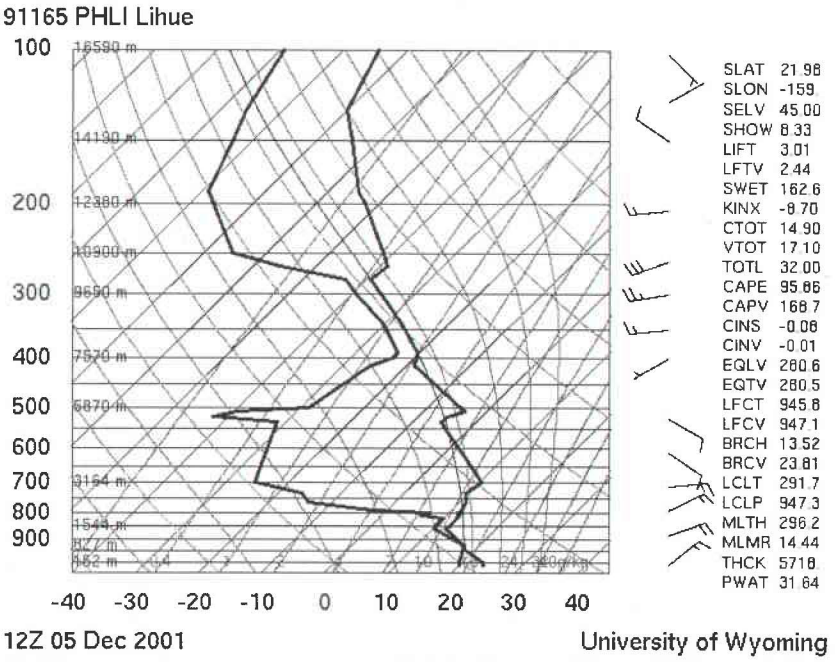

Figure 3-2: Observed sounding from Lihue for 0200 HST 5 December 2001

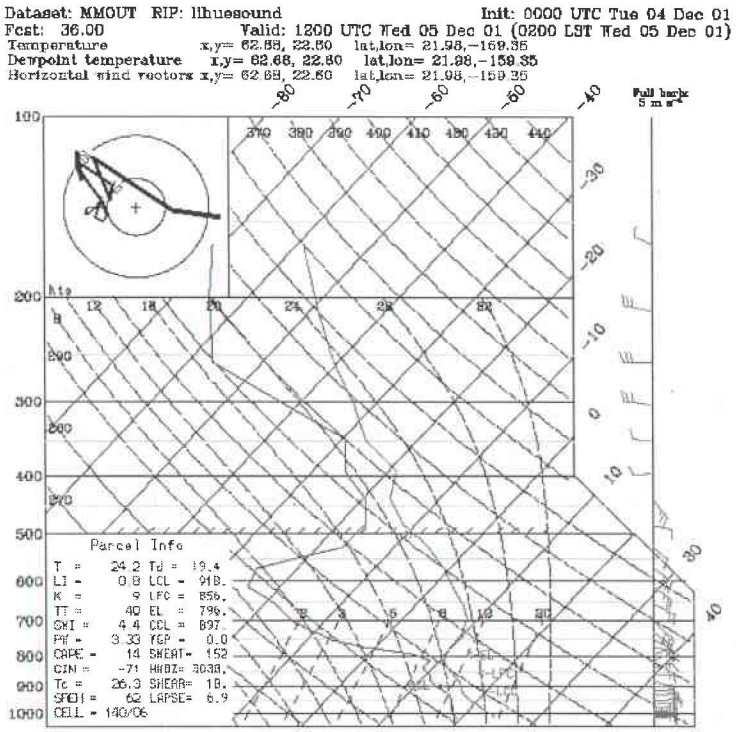

Figure 3-3: Model sounding at the same location as the Lihue sounding, for 0200 HST 5 December 2001.

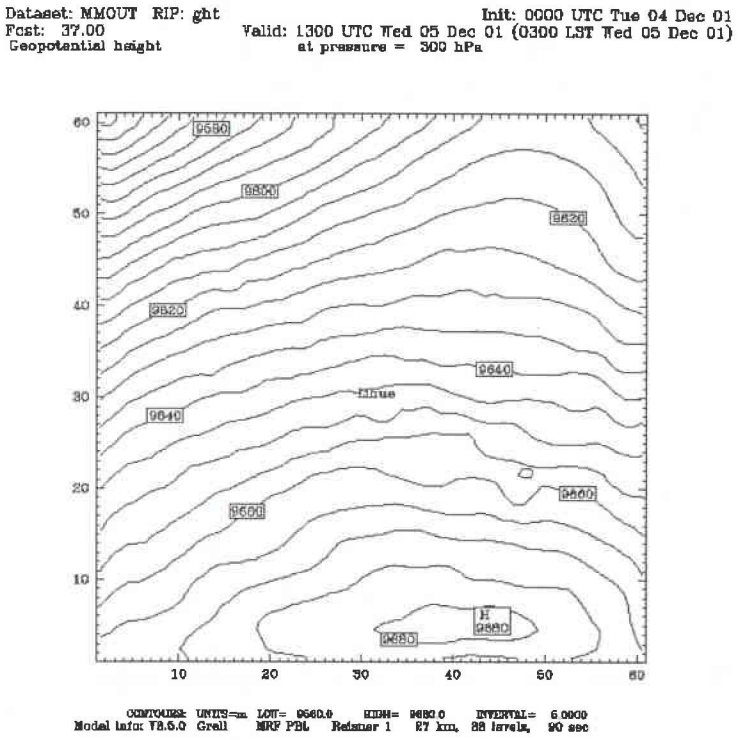

Figure 3-4: Modeled 300 hPa geopotential height for domain 1 at hour 37 (0300 HST on 5 December). Contour interval is 5 meters. Kauai is in the center of the domain. Grid marks on the side are for model grid points, so the number 10 stands for 270 km.

3.3 Model rainfall:

The first 12 hours of all simulations are considered a spin up period; therefore only the rainfall during the latter 60 hours of the simulations is examined. All references to rainfall will be referring to modeled rainfall unless stated as observed rainfall. References to observed rainfall will refer to rainfall observed at the Hydronet stations and the Mt Waialeale rain gauge. Here follows a brief description of the 1 hourly rainfall for domain 4.

In this simulation most of the rain over the island fell between hours 17 to 27 (0700 to 1700 HST on 4 December). During hours 17 to 21 (0700 to 1100 HST) rainfall occurred over northwest Kauai. Hours 22 to 27 (1200 to 1700 HST) produced rainfall

over the mountain areas particularly over and to the south of W. The largest 1 hourly total was 19.5 mm. This amount occurred on two occasions during the hours leading up to hours 22 and 26 (1200 HST and 1600 HST on 4 December). Both of these maxima occurred over the summit region of W. Observations of rainfall at the Waialeale rain gauge (Fig. 3-5) show that rain fell mainly between 15-min periods 49 and 85 (hours 12.25 to 21.25 → 0215 to 1115 HST on 4 December). Thus although the simulation agrees with the general focus of rainfall in the earlier part of the period, the timings of the main rainfall are not in agreement with observations.

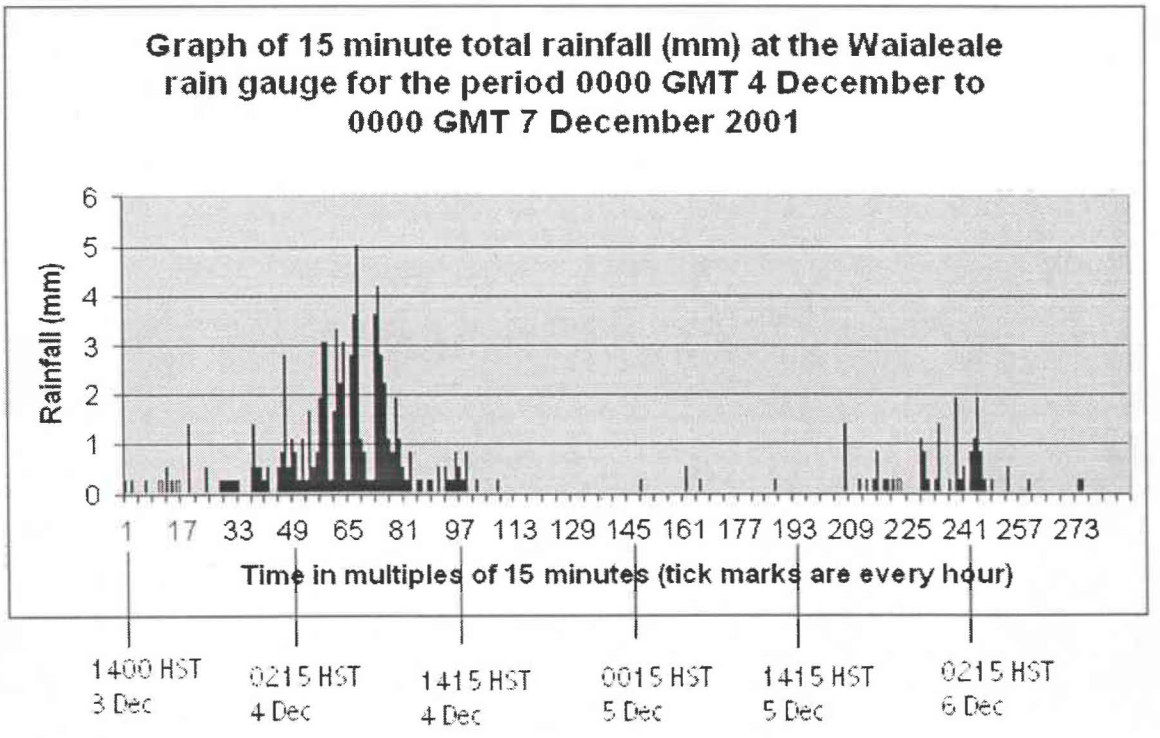

Figure 3-5: Observed rainfall at the Mount Waialeale rain gauge for the period of the Easterly wind simulation. Values represent 15 minute totals in mm.

The total modeled rainfall and the rainfall observations for the last 60 hours (0200 HST on 4 December to 1200 HST on 6 December) of the simulation (ignoring the first 12 hours as they lie in the spin up period) are shown in Figure 3-6. This figure reveals enhancement of rain over the mountains. The largest total rain lies over W where the model generated 150 mm of rain. This is 54 mm more rain than observed at the Waialeale rain gauge where 96 mm was recorded. The Hydronet observations for this case reveal how much drier other areas of the island were during this period. The model qualitatively agrees with these observations. The model produces approximately 5 to 15 mm more rain than observed over the 4 easternmost Hydronet stations. The 2 northernmost stations record about 15 to 20 mm more rainfall than the model predicts. Kokee, the most western station records the lowest total of 5 mm, agreeing with the model results. The southernmost 3 stations agree with the model results that the middle station has the most rain, however the stations either side observe less rainfall than predicted by the model. This may be related to orographic forcing by the smaller mountains in this region that are poorly resolved in the model terrain.

The modeled total rainfall over this case produces encouraging gradients in rainfall across the island. 150 mm of rain at W is about 10 times more rain than the 15 mm of rain modeled along the eastern coast. Observations of 7 and 6 mm of rain at the stations near the coast when compared with the 96 mm observed at W suggest a similar, if perhaps larger, gradient in rainfall in reality. The lack of significant rainfall over the western coast agrees with expectations but there is a lack of observations in this area to directly compare. Given the approximations in the model and the errors associated with

rain gauge measurements, the rainfall gradients appear to be in reasonable agreement with observations.

Comparing Figure 3-6 with the mean annual rainfall on Figure 1-2 reveals similarities in the overall rainfall distribution produced by the model with the annual rainfall. Kauai annual mean rainfall distribution is dominated by trade wind rainfall (Lyons 1982). This dominance leads to greater rainfall over the windward mountains, in both Figure 3-6 and Figure 1-2, than over leeward areas at a similar elevation. Over only 3 days of modeled trade wind rainfall the distribution characteristic of a much longer time period has become evident. This encouraging sign suggests that the model is performing well at producing trade wind orographic rainfall. Also of note is that this simulation is specifically one of winds from a more east direction than that of typical trade winds. The rainfall totals in this simulation along the northern and southern coasts, which lie roughly parallel to the wind direction, are similar. In contrast the mean annual rainfall tends to have more rainfall over the northern coast associated with the more dominant northeasterly wind direction.

If we were to consider a situation in which a year's weather consisted simply of this case repeating itself over and over again, then the total rainfall at the summit would be about 18,000 mm and the rain along the eastern coast would be about 1800 mm.

Overall the model produces an apparently realistic distribution of rainfall across the island for this case. This is an important conclusion that suggests that the model can be used with some confidence to establish in detail the processes that are leading to the rainfall distributions over Kauai.

Over the period of this simulation there was some evidence of thermally driven diurnal circulations however because of the variable nature of the trade wind layer and the short length of the simulation it is difficult to conclude how diurnal circulations affected the wind patterns over the island. The model suggests that underneath the conditions of this case the land and sea breeze circulations were generally damped or overrun by the trade wind flow making them weaker or less apparent. Modeled down-slope flow did develop on some windward inland areas on the early mornings of the 4, 5, and 6 December however this flow did not propagate past the coastline. It is possible that daytime upslope flow aided ascending air above windward slopes but there is not clear evidence of this in this simulation. There was no obvious diurnal pattern in rainfall and so it is unclear how rainfall at W could be influenced by either the island induced diurnal forcing or the large scale open ocean diurnal forcing.

Precipitable water over the open ocean was 30 to 60 mm over the open ocean for this case and 10 to 30 mm over W (not shown). Part of this reduction in precipitable water will be associated with the removal of moisture through rainfall and part of it will be associated with the divergence of low level moist air over the island. There is not a clear difference in precipitable water between the windward and leeward coasts. This suggests that the removal of water through rainfall over the mountains may not be the key factor that is inhibiting rainfall over lee areas. Descending air and the associated advection of dry air from aloft appear to be more important in reducing leeward rainfall. This will be discussed further in section 3.4.3.

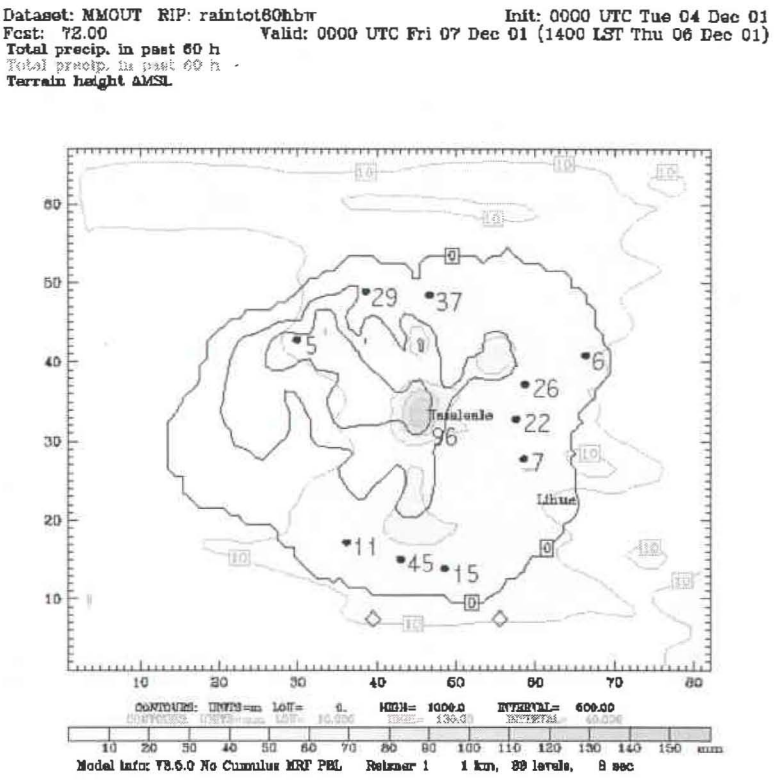

Figure 3-6: 60 hour total modeled rainfall (mm) for the easterly wind simulation. Excludes the first 12 hours. The light shaded lines are isohyets plotted at 40 mm intervals starting at 10mm. The dark lines are contours for height above sea level are given for 0 meters, 500 meters, and 1000 meters. The maximum rainfall is 155 mm. The numbered dots show the rainfall observed at the Hydronet stations over the same time period.

3.4 Cross-sectional analysis:

For all simulations vertical cross sections across the island were plotted. The main variables plotted were: wind vectors, cloud water, potential temperature, relative humidity and equivalent potential temperature. The purpose here is to gain a better picture of the processes that lead to the large orographic rainfall totals and gradients. To do this I will focus on a particular period of modeled heavy rain over W. As mentioned in the previous section there was a period of persistent rain over the summit between hour 25 and 26 when 19.5 mm of rain was modeled. This is shown in Figure 3-7. The cross section used for this case was the east to west cross section across the island shown in

Figure 3-8. The hours 24 to 27 (1400 to 1700 HST 4 December) will be examined in the following section.

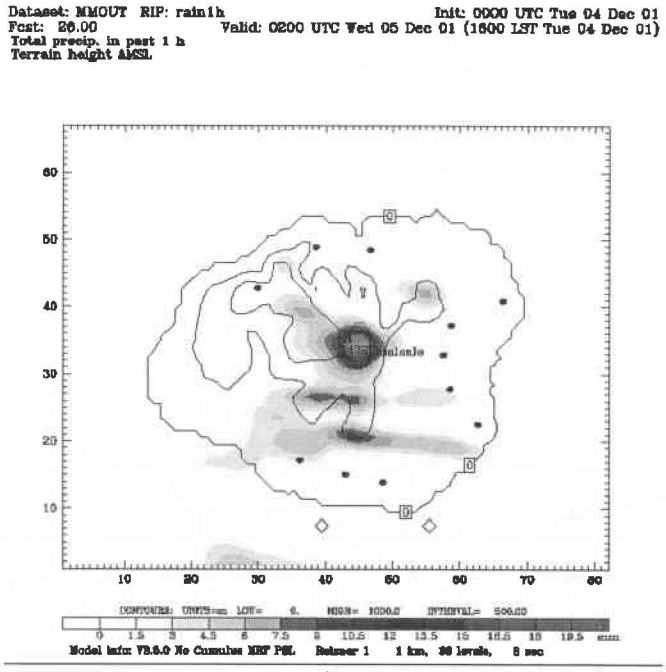

Figure 3-7: Total 1 hour modeled rainfall between hour 25 and 26 (1500 to 1600 HST on 4 December 2001) in mm.

3.4.1 Modeled rainfall during hours 24 to 27 (1400 to 1700 HST on 4 Dec 2001) – A modeled afternoon orographic rainfall event

Over this afternoon period 30 mm of rain fell at W. Rain fell over the mountainous areas of the island but no rain fell along the western coast. No rain fell on the northern or northeastern coast; therefore no rain fell over the coastal region directly upwind from W. The only rain at the coast fell over the southern coastal regions.

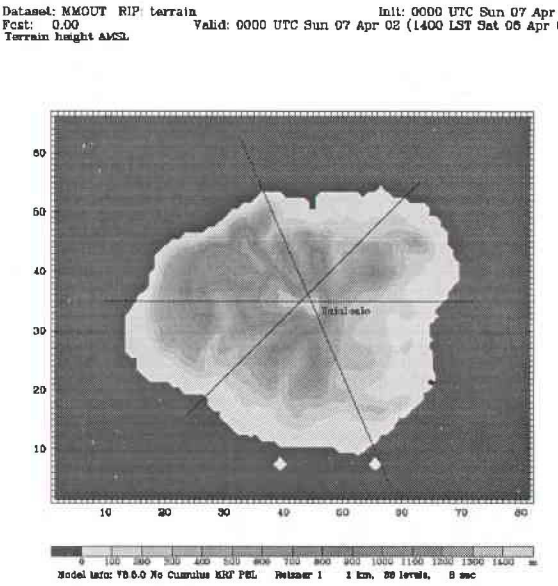

Figure 3-8: Same as Figure 2-3 but including lines that show where the cross sectional analyses were taken. The line oriented east to west was used for the easterly wind case. The line oriented southwest to northeast was used for the light southwesterly wind case, the shear line case, and the strong northeasterly wind case. The remaining line oriented northwest to south east was used for the 1995 kona low simulation. Cross sections were chosen to lie roughly parallel to the average surface wind direction over the period of each simulation.

3.4.2 Cross sections of cloud water, potential temperature and wind vectors for hours 24-27 (1400 to 1700 HST on 4 December):

Cross-sectional analysis for hour 24 (1400 HST) shown on Figure 3-9:

At this time the model simulates low level winds blowing from east to west along the axis of the cross section. The wind vectors suggest that air is ascending over the eastern slopes of W. The region of strongest ascent lies adjacent to the steepest slopes just east of the summit crest. This region of strong ascent is about 4 km wide in an east west direction at 1500 m elevation. Above the summit crest there is a transition from upward motion to downward motion. The downward motion continues as down-slope winds down to the Waimea Canyon region. Descending motion is strongest just west of the summit crest; in fact there is a transition from 3 m s^{-1} ascending air to 2 m s^{-1}

descending air over the space of just 2 to 4 km across the summit crest at 1500 m elevation.

Cloud water shown as shades of grey on Figure 3-9 is used to visualize the presence or absence of clouds. At hour 24 thin cloud (about 300 m thick) lies over the Lihue Basin. Near the steep windward slopes of W the cloud is deeper, about 1500 m thick. The cloud base over the windward slopes is at 800 m. Orographic cloud lies over the summit but stretches only 7 km down the leeward slope. The cloud base is higher on the leeward slope at 1200 m.

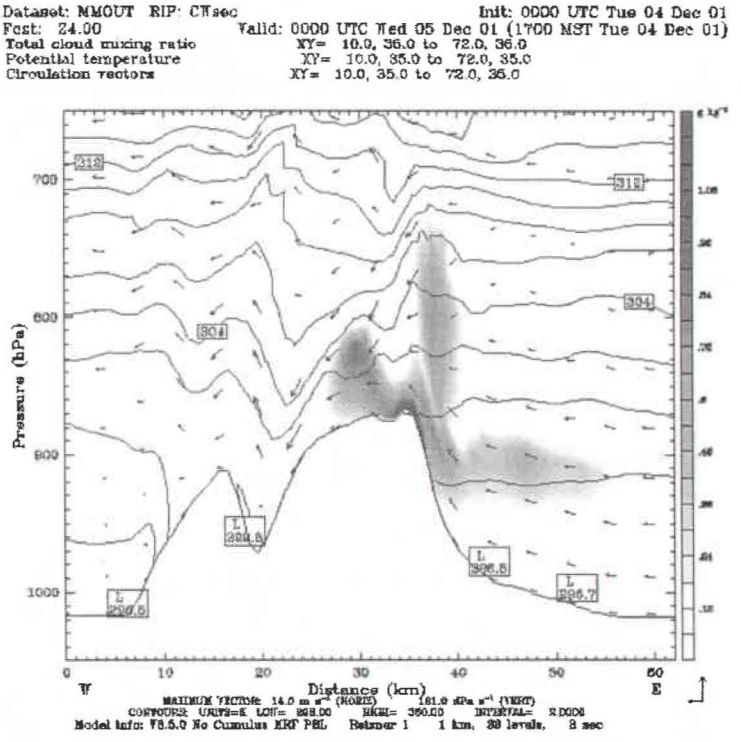

Figure 3-9: Cloud water (shades of grey in g kg^{-1}), potential temperature (contours °K), and wind vectors (in the plane of the cross section) for hour 24 of the simulation (1400 HST 4 December 2001). A wind vector with a horizontal component long enough to reach the start of the next vector would represent a horizontal wind speed of 40 m s^{-1}. The maximum magnitude of a vertical velocity vector component is 18 Pa s^{-1} in this cross section. The maximum vector components in the horizontal and vertical are indicated in the bottom right of the figure. The cross section used here is west-east cross section across Kauai looking north. The lowland to the east is the Lihue basin. The highest point marks the Mt Waialeale region. The valley towards the west is the model resolved Waimea Canyon.

Analysis for hour 25 (1500 HST) shown on Figure 3-10:

At this time an area of cloud 2000-3000 m deep lies over the Lihue basin. It is this region of cloud that produces the 19.5 mm of rain over the following hour over W. This cloud produced no rain over the coast east of W suggesting that it probably developed on approach to the mountain. The development of the cloud over the Lihue Basin is only partly associated with the orographically forced ascent over this region. The strong ascent within the cloud suggests that the region of general ascent is being significantly enhanced by moist processes within the cloud itself. Orographic ascent to an air parcel's LCL triggers condensation and therefore latent heat release. The added buoyancy will be further enhancing upward motion within the cloud, aiding rapid development. Thus as well as orographic lifting, moist processes will play a key role in the development of the cloud on approach to W.

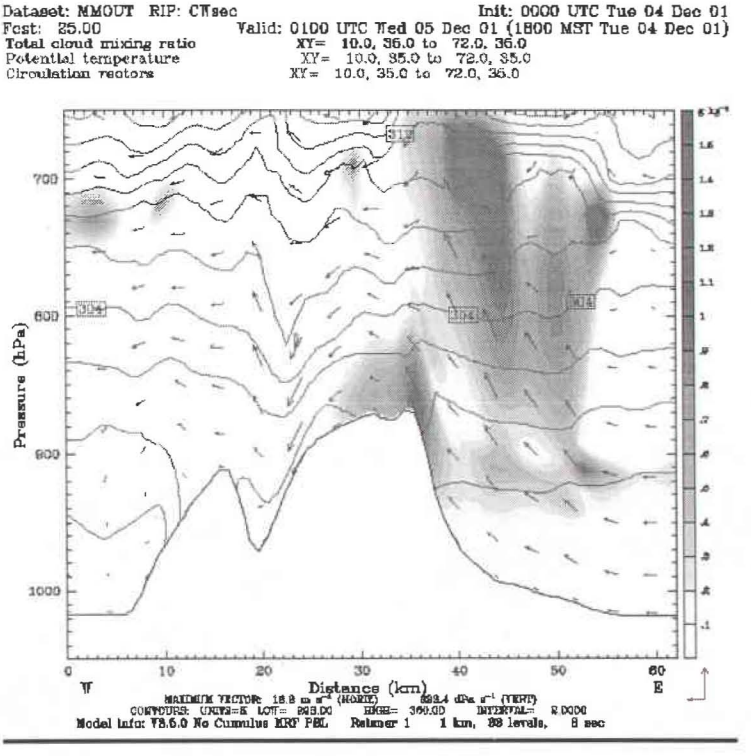

Figure 3-10: As Figure 3-9 except for hour 25 (1500 HST 4 December). Maximum vertical velocity component is 23 Pa s^{-1}.

Analysis for hours 26 and 27 (1600 and 1700 HST) shown on Figures 3-11 and 3-12:

Given an approximate wind speed of 10 m s^{-1} we would expect the thick cloud mentioned for hour 25 to have moved around 30 to 40 km towards the west. The cloud just west of the Waimea Canyon region of the cross section at hour 26 (Fig. 3-11) is therefore probably associated with the previously thick cloud region. The cloud over the Waimea Canyon is less deep and less wide than the cloud upwind at hour 25. Upwind of W cloud continues to deepen on approach to W. Thick orographic cloud persists over W and the cloud base is lowest close to the windward slope surface. At hour 27 only thin clouds exist upwind of W; however the orographic cloud remains.

General features for the entire case

For every hour in this simulation cloud was present over the summit crest of Waialeale. This does not imply that there were no simulated cloud free periods over W but that at each hourly snapshot, cloud was present. This persistent orographic cloud formed because air parcels were at all hours rising up windward slopes to their lifting condensation level that lay at around 1000 m elevation. This fact suggests that for each hourly snapshot of the simulation uplift on the upper windward slopes of Waialeale was aided by latent heat release.

Though this cloud was persistent, significant rain appeared to fall only when there had been upwind cloud present over the previous hour. Upwind cloud in general tended to thicken and deepen between the coast and Waialeale. The cloud base tended to be lowest near to the steep windward slope of Waialeale.

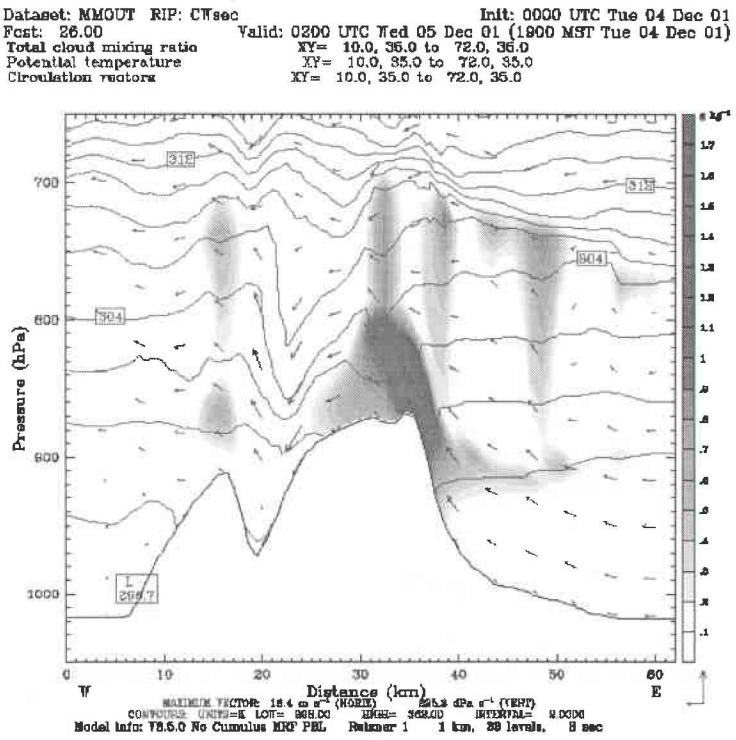

Figure 3-11: As Figure 3-9 except for hour 26 (1600 HST 4 December). Maximum vertical velocity component is 24 Pa s^{-1}

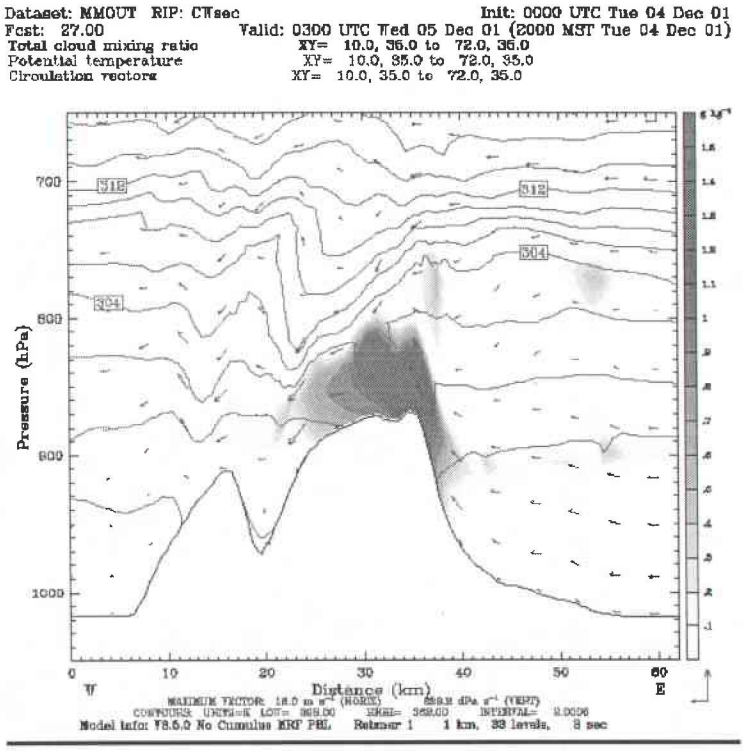

Figure 3-12: As Figure 3-9 for hour 27 (1700 HST 4 December). Maximum vertical velocity component is 23 Pa s^{-1}.

3.4.3 Relative humidity and equivalent potential temperature hours 24 to 27:

Plotting relative humidity (RH) helps to reveal the depth of the trade wind moist layer. At the top of the moist layer there is usually a large gradient in humidity between the moist layer below and the large-scale descending dry air aloft. Equivalent potential temperature is conserved in a moist adiabatic process and can therefore be considered an approximate tracer of an air parcel that is saturated.

Figures 3-13 to 3-16 reveal how the moist layer evolved over this period of rainfall. These figures reveal that the moist layer structure is affected by the island in a number of ways. Over these hours and over the simulation period the leeward side of the island tended to have lower average RH within the moist layer. Here we will consider the moist layer top as the level where there is a rapid decrease in humidity of air with height above the moister air below. Specifically I will use the 50% RH contour as an approximate moist layer top in this simulation.

The height of the moist layer top was related to the presence of clouds. For example the deepening of the moist layer between hour 24 and 25 (Figs. 3-13 and 3-14) was related to the development of clouds over windward Kauai. The tendency for clouds to deepen on approach to W corresponded to a lifting of the moist layer top by a few hundred meters. At lower levels, approximately 950 hPa and below, there was a slight increase in RH from the coast to the point where the level intersects the mountain. For example at hour 26 (Fig. 3-15) the 980 hPa RH increased from 80% at the coast to 90% 15 km inland. Low level RH increases were associated with the advection of low level moist air upslope. Higher RH implies a lower LCL near windward slopes than over the

east coast. This would explain the lowering of cloud base near windward slopes of W, described in section 3.4.2.

The moist layer structure is also affected downwind (west) of W. Over the crest of the mountain the upward moving air changes to downward moving air. The precise location of the transition varies throughout the simulation. There is also a variation in vertical motion with height over W. Upward motion within the moist layer above W often lies below descending motion near the moist layer top. Above the lee slopes of the island down-slope flow near the surface and descending motion aloft tend to advect dry air from aloft downwards. This can be seen most clearly at hour 24 (Fig. 3-13) and hour 27 (Fig. 3-16) The drying of the air over leeward areas is therefore likely to be a combination of this dry advection from aloft as well as moisture removal through rainfall over the mountains. Equivalent potential temperature contours cross RH contours (from more humid to less humid) on the lee side of W suggesting that moisture is being removed from this air through rainfall. The vertical mixing not only tends to dry the moist layer but also tends to reduce the gradient in RH at the moist layer top. As a consequence the air at elevations near the moist layer top, for example at 700 hPa, can often have a higher RH over the leeward coast than over the windward coast. This is the case for the four hours shown in Figures 3-13 to 3-16.

For this time period the flow of the moist layer over W produces a dramatic change in moist layer depth. Over the windward coast the moist layer was between 250 and 300 hPa thick. The lifting of the moist layer top combined with the gradual rise in elevation leads to a similar moist layer thickness at the western end of the Lihue Basin. Even though the moist layer top rises between the Lihue Basin and W the large rise in

surface elevation leads to a drop in the moist layer thickness leaving it just 100 to 250 hPa thick over W. The implied reduction in moisture content of the column between the Lihue Basin and W could be due to rainfall moisture removal and/or divergence of the flow. Over lee slopes between W and the Waimea Canyon there is large variation in moist layer thickness of between 80 and 200 hPa because of the temporal variability of downward dry air advection.

The descending air below the moist layer top continues down to the eastern side of the Waimea Canyon throughout this time period. Over the Waimea Canyon region there is then a transition to rising motion. This pattern is similar to that of a hydraulic jump that Lavoie (1974) suggested existed on the leeside of the Koolau Mountain Range on Oahu. In this case however it is also clearly related to the air rising over the high ground to the west of Waimea Canyon. On the lee side of the high ground to the west of Waimea Canyon there is a transition back to descending air. For periods of this simulation there is then evidence of a secondary dry intrusion and a secondary hydraulic jump that occurs between the western high ground and the western coastline. A weak example of this can be seen on Figure 3-16.

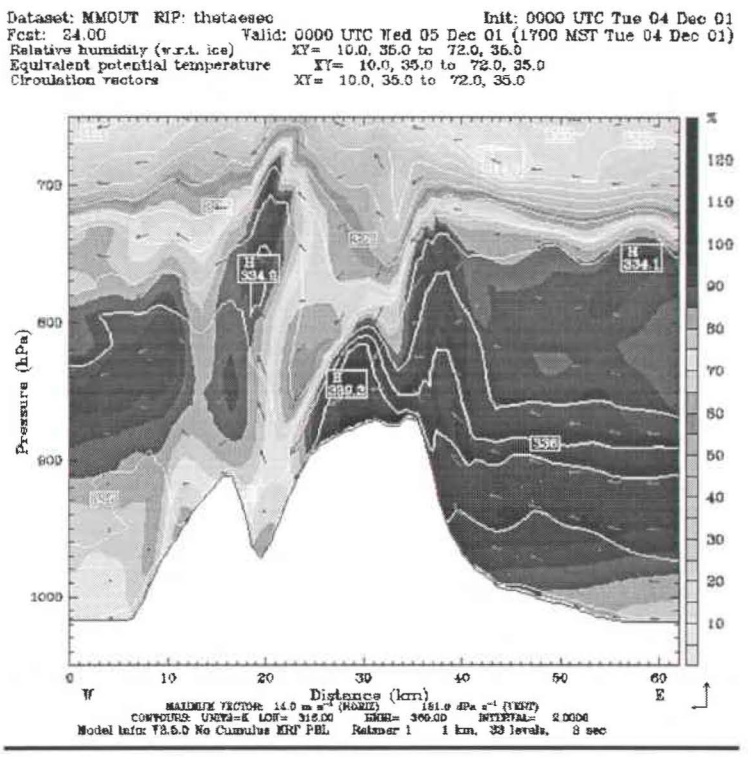

Figure 3-13: The same cross section for hour 24 (1400 HST 4 December) as Figure 3-9 but now showing relative humidity (shades %, contours every 5%), equivalent potential temperature (white contours every 2 K), as wind vectors (in the plane of the cross section).

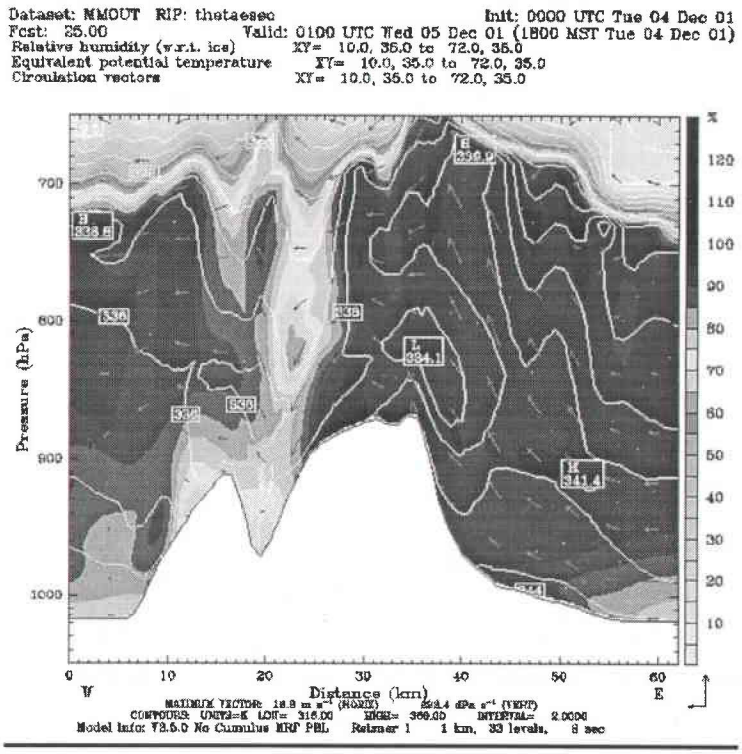

Figure 3-14: As Figure 3-13 for hour 25 (1500 HST 4 December)

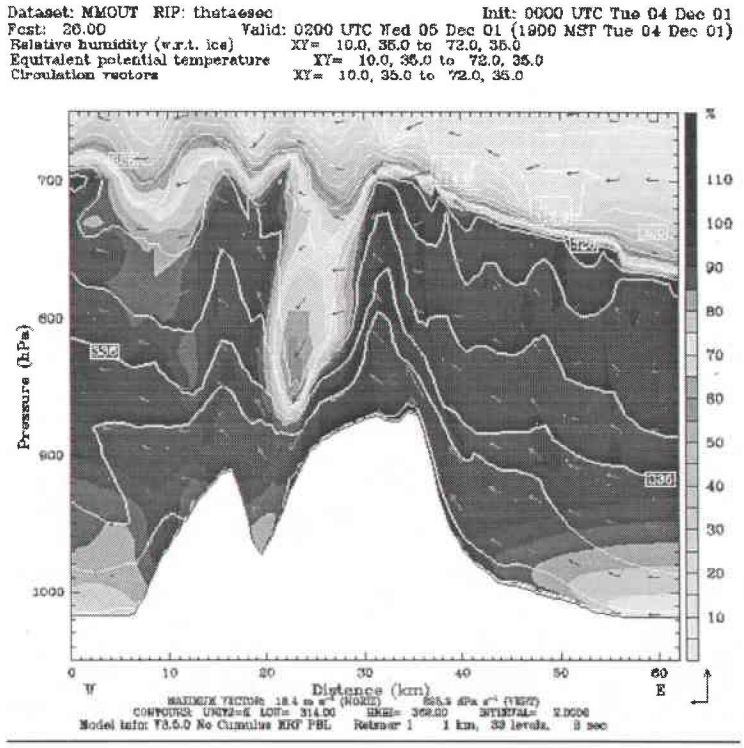

Figure 3-15: As Figure 5-13 for hour 26 (1600 HST 4 December)

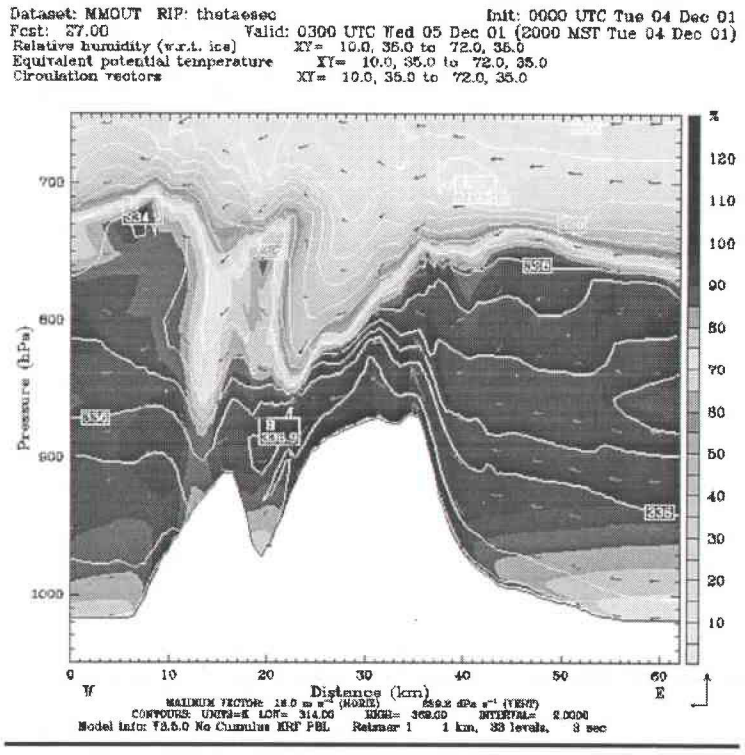

Figure 3-16: As Figure 3-13 for hour 27 (1700 HST 4 December)

3.4.4 Trajectories hours 24-27:

The equivalent potential temperature contours of Figures 3-13 to 3-16 suggest that low level air is advected over the top of W. Back trajectories plotted from points directly above W help corroborate this conclusion as shown on Figure 3-17. Figure 3-17 shows that air from near the surface of the Lihue Basin was advected up and over the top of W at this time.

Plotting many equally spaced 3d forward trajectories in the cross section for hour 25 to 26 confirms the dominance of flow over rather than around the island as shown in Figure 3-18. This pattern prevails throughout hours 24 to 27 however other periods show a different pattern. Before hours 24 to 27 there tended to be greater flow around the island rather than over it as shown for hours 16 to 17 in Figure 3-19. Three possible

reasons why we see this marked difference in flow patterns are: 1) Hour 16 (Fig. 3-19) is at 0600 HST in the morning therefore the nocturnal flow associated with nighttime island cooling may be interacting with the large scale flow and affecting the flow of air over the island. 2) The open ocean wind speed is approximately 7 m s^{-1} at hour 16 whereas it is about 10 m s^{-1} at hour 25. This indicates larger Froude number flow at hour 25 that would suggest greater flow over the obstacle rather than around it. 3) Larger orographic clouds present during hours 25 to 26 will be aiding uplift through latent heat release and this therefore may be aiding flow over the mountains.

The differences between Figures 3-18 and 3-19 suggest that the flow over W is variable under trade wind conditions. The different factors that may be responsible for these flow changes require further investigation (see section 6.1). The orographic rain event looked at in this section is one example from an afternoon period however the principal features seen in this period apply to other periods of orographic rain in this simulation.

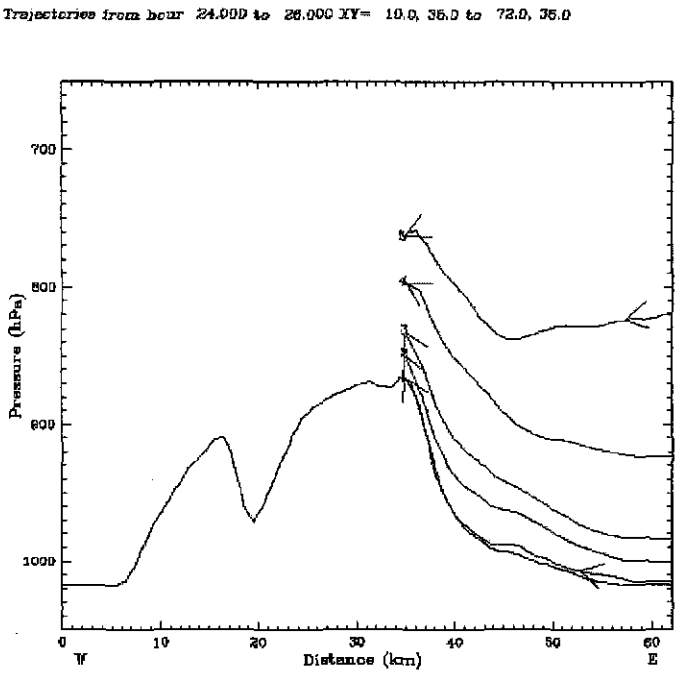

Figure 3-17: Three dimensional (plotted in a 2 dimensional frame) 2 minute back trajectories shown in the same cross section as Figure 3-9. Back trajectories are interpolated from 1 hourly data and are started at different heights above the highest point in the cross section.

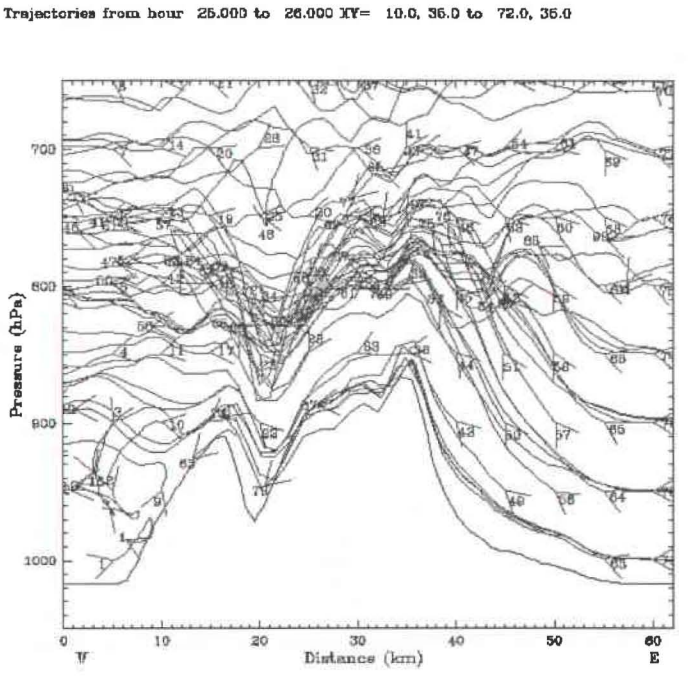

Figure 3-18: 2 minute three dimensional forward trajectories interpolated from 1 hourly data for the period between hours 25 and 26. The trajectories start from points in the cross section that are 5 km apart in the horizontal and 50 hPa apart in the vertical.

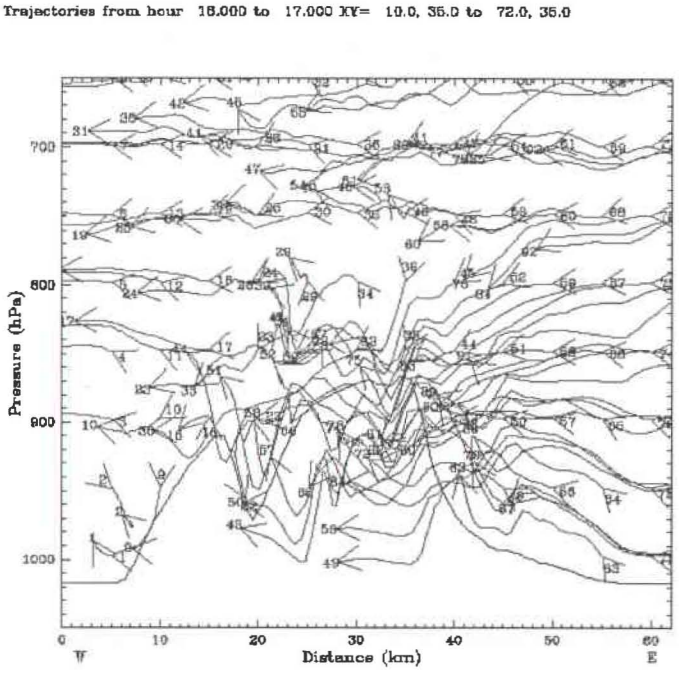

Figure 3-19: As figure 3-18 but for the period between hours 16 and 17

3.5 Overall

The accurate simulation of rainfall in this case suggests that it may be replicating trade-wind orographic rainfall realistically. The moist layer top rises over windward slopes associated with flow over the island combined with latent heat aided uplift in developing clouds. The high Fr flow (Fr = 0.66), inversion forced strong down-slope winds (Durran 1986) and evaporative cooling (Hall 1980) are likely to be important in initiating the downward motion on the lee side of the island. This transition from upward to downward motion over W is important in triggering the "mini cloudburst" of rainfall suggested in Ramage and Schroeder (1999). The height of W in relation to the typical trade-wind moist layer top is, through evaporative cooling and inversion forced down slope flow, probably important in determining the strength of the vertical motion

transition over W and thus focusing persistent rainfall over W. A mountain height of around 1500 m and a typical trade wind layer top of between 2000 and 3000 m may be close to optimum for rainfall generation at the summit. Hawaiian islands with peak elevations in between 1700 and 2500 m that might focus more trade-wind rainfall at their summits do not exist for comparison; however they could be modeled (see section 6.3). The shape of W is also likely to be important with the steep eastern facing slopes of W aiding strong uplift of air and rapid cloud development just upwind of W.

4 Other Case Studies

4.1 Case 2: Weak southwesterly winds of 7 to 10 April 2002

4.1.1 Background:

This case covers a period when the islands were under a light wind regime. The winds were from a southerly or southwesterly direction. Winds were therefore Kona (leeward) winds, therefore the leeward coast lay upwind for this case. The surface pressure analysis for 0000 GMT on the 9 April is shown on Figure 4-1.

At the start of the simulation period, 0000 GMT, 7 April a cold front lay about 200 km to northwest of Kauai. This front was associated with a large weak (1000mb) low pressure system centered at 160°W, 40°N. A large high pressure elongated in a north south direction lay centered to the northeast of the islands at 135°W, 37°N. A ridge stretching out from this high reached over the Big Island. Throughout the simulation this ridge lay over, or near the Big Island and therefore southeast of Kauai. It was this pattern that led to the persistent Kona winds over Kauai. The front dissipated before it reached the islands and the eastern low pressure system moved towards Alaska. By 0000 GMT on 9 April the high pressure lay centered at 128°W, 28°N and a new low pressure system lay to the northwest of Kauai centered at 170°W, 35°N as shown in Figure 4-1. There was little change in this pattern near the islands for the remainder of the simulation. Thus Kauai lay under the subtropical ridge in subsiding air ahead of the cold fronts for the period. A crude calculation of the Fr for this case of roughly 5 m s^{-1} large-scale winds gives Fr = 0.33 (using N = 0.01 s^{-1} for consistency with previous studies, and h = 1500 m).

The model soundings over Lihue showed a conditionally unstable layer from the surface to usually between 800 and 900 hPa. This layer was generally shallower than for case 1 and was capped by a stable layer that contained a weak inversion during the latter half of the simulation. CAPE was 0 J kg^{-1} in the model throughout the simulation. The average K index for the 6 hourly soundings was 11 corresponding to a near 0% probability of air mass thunderstorms.

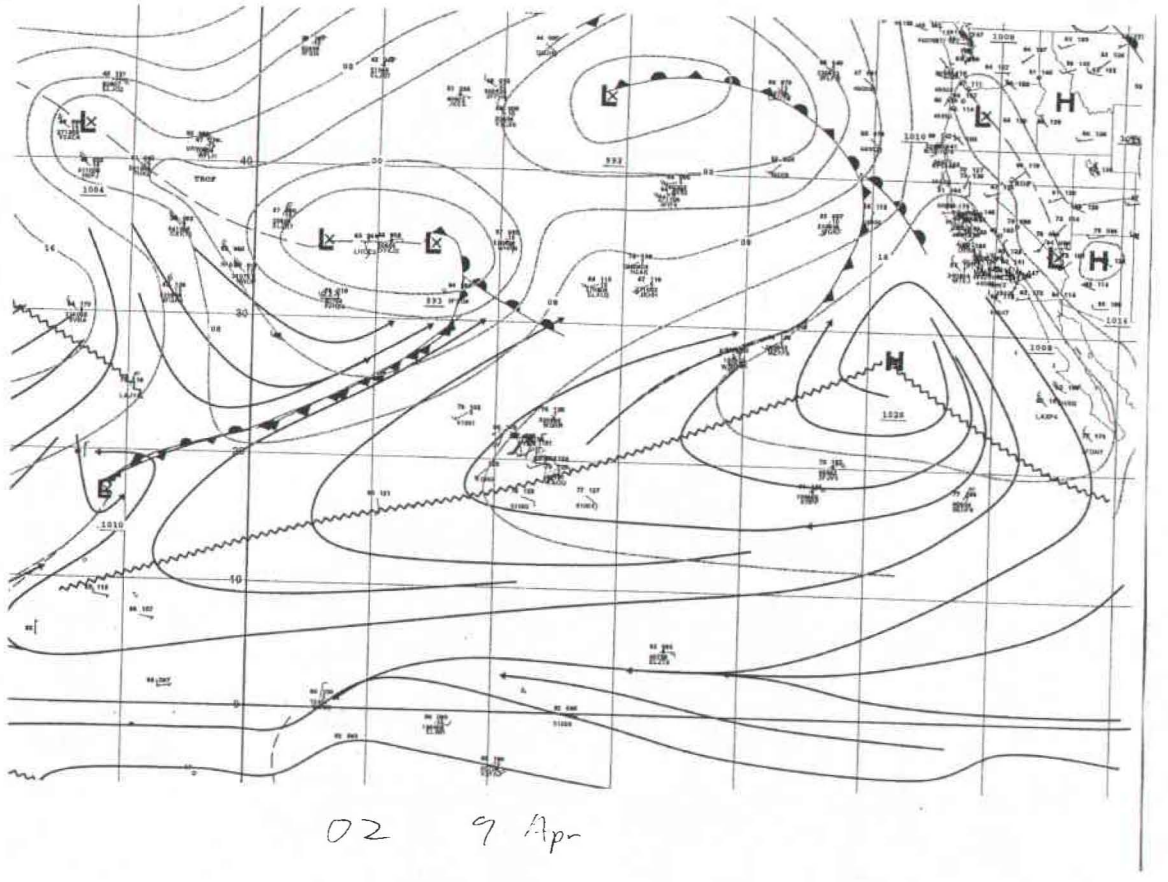

Figure 4-1: Surface pressure analysis for 0000 GMT 9 April (1400 HST 8 April)

4.1.2 Rainfall:

Over the 72 hours of the simulation there was very little rainfall. Total rainfall over land exceeded 10 mm over a small region of the southern coast and over two small regions inland, one over the Alakai Swamp area and the other over the ridge to the west of the Waimea Canyon. No rain was simulated over W and no rainfall was observed at the rain gauge. The largest rainfall total of over 20 mm within the 1 km resolution domain occurred offshore to the northwest of the island. This maximum appears to be associated with a region of convergence formed by winds accelerating around the northwest of the island converging with the large scale flow. Most of the rain fell here during hours 41 and 42 (0700-0800 HST 8 April). At this time southerly surface winds of around 10 m s^{-1} were modeled around northwest coasts. This wind was more a consequence of a stronger wind event that originated out of the southwest corner of the domain and propagated around the northwest side of the island. This is likely a consequence of a serious model irregularity that will be discussed in chapter 6.1. Light rain was modeled (1-3 mm h^{-1}) over various small areas of southern Kauai in the evening of 7 April (1700 HST and 1900-2100 HST) and the morning of the 8 April (0000, 0300, 0400 and 0800 HST). The heaviest rain over southern Kauai (approx. 10 mm h^{-1}) occurred over a small region near Hanapepe between 0300-0500 HST on 9 April. The rainfall simulation is successful in the sense that it produced very little rain and that agrees with the observations over this period that recorded little or no rain.

There was less precipitable water for this case than for case 1. The precipitable water over the open ocean was 20-40 mm and over W was 5 to 20 mm. The shallow moist layer of this case largely explains these low values. Given that there was virtually

no rainfall over this period it is clear that divergence of low level moist air around, rather than over W is responsible for the difference in the precipitable water between the open ocean and W.

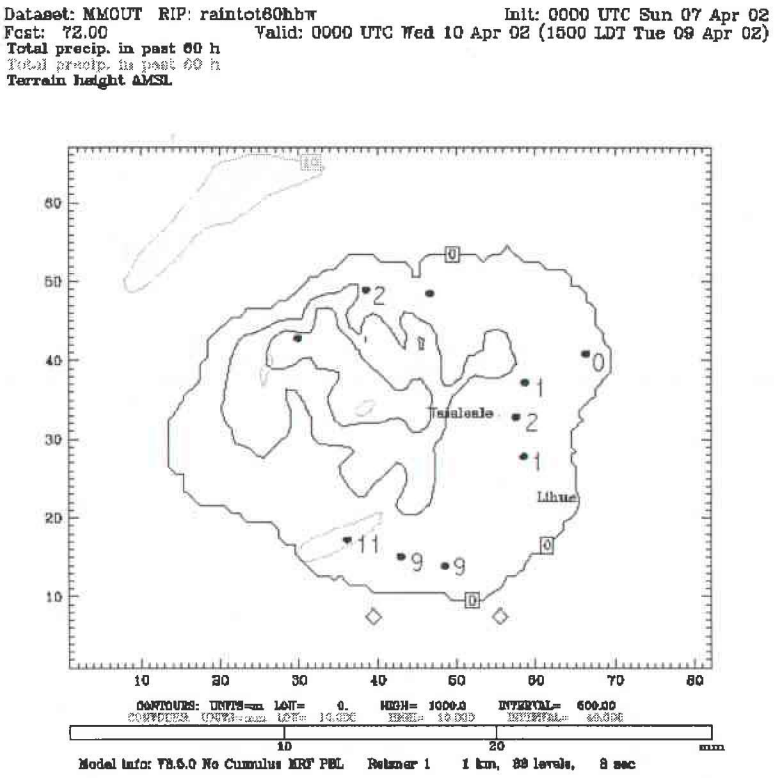

Figure 4-2: Total modeled rainfall, excluding the first 12 hours for the weak south westerly wind case, in mm.

4.1.3 Surface Wind

The light winds open ocean winds of this simulation enabled island thermally forced diurnal circulations to become clearer. During the daytime onshore flow was most prevalent as can be seen in Figure 4-3 over windward areas and in the wake of the island (northeast coast). Onshore flow developed rapidly over southern coasts between 0800 HST and 1000 HST on the 7, 8, and 9 April. Onshore flow also developed in the calmer

wake region on the north and northeast coast in the mornings. Kona winds, perhaps aided by the sea breeze, dominate the winds over the majority of the island, with the exception of the wake region. Flow deflection around the island associated with the lower (in relation to the easterly wind case) Froude number of this case causes flow acceleration around the flanks of the island. In the wake region the light (< 5 m s^{-1}) onshore northerly or northwesterly flow dominates approximately one sixth of the island in the north or northeast of the island during the day. The position of this wake region depends on the large-scale wind direction. Consequently as the wind direction shifts from a southwesterly direction to a more southerly direction over the course of the simulation, the wake region shifts from the east to the north of the island. The calmer winds of the wake region continue clearly for about 90 km downwind of the island.

During the nighttime down slope and offshore flow occurred over many areas of the island. This was most evident in the Waimea Canyon region where down valley flow developed on all three nights of the simulation. This down valley flow combined with general offshore flow had propagated 5-10 km off the southern shore at 0000 HST on 9 April (not shown). Figure 4-4 shows the flow 3 hours later with the offshore flow closer to the coast. In the wake region of the island the flow direction became variable during the night with a tendency for either weak offshore flow or easterly flow along the coast.

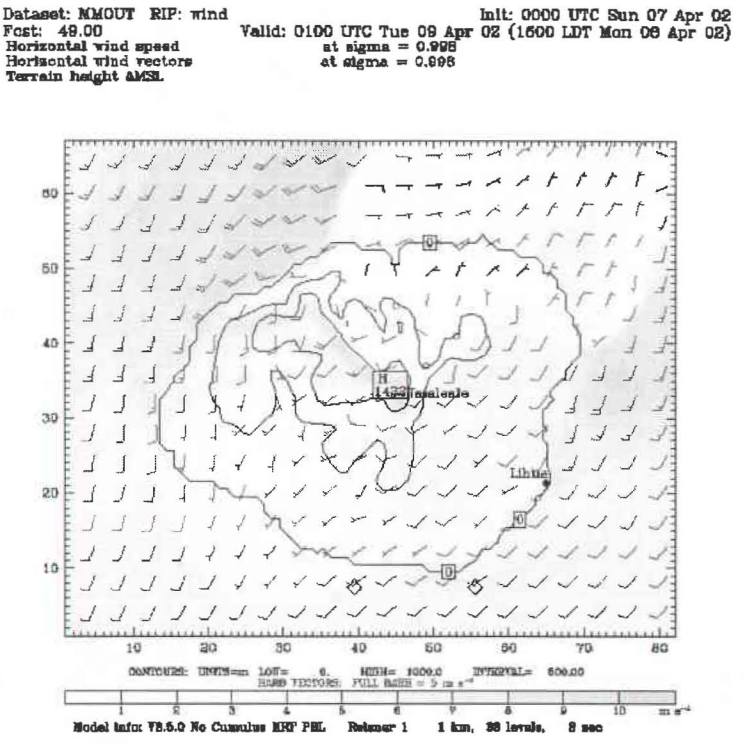

Figure 4-3: Surface wind speed (shades in m s^{-1}) and wind direction (barbs) for hour 49 (1500 HST 8 April 2002).

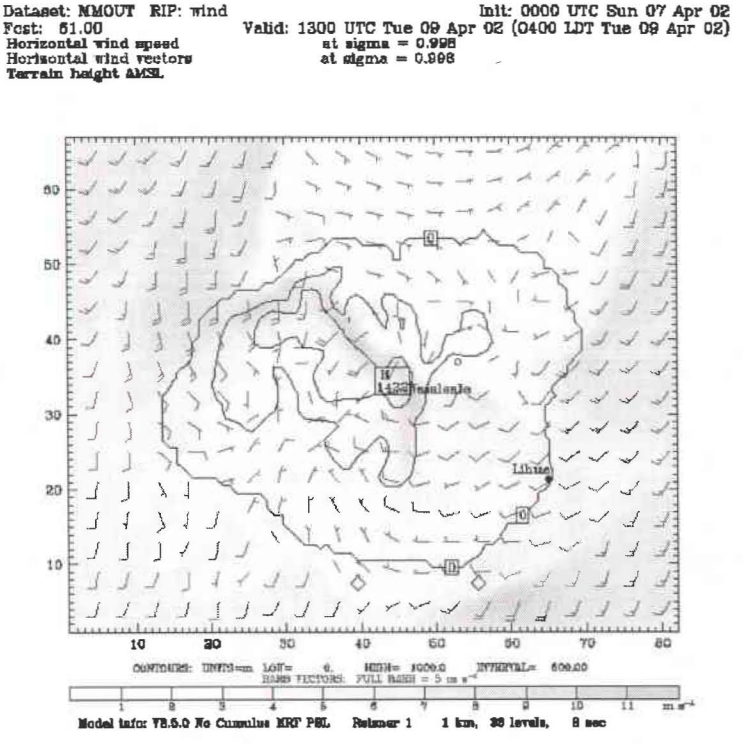

Figure 4-4: As Figure 4-3 but for hour 61 (0300 HST 9 April 2002)

4.1.4 Cross section analysis

This case was characterized by a shallow moist layer throughout the simulation. Typically the moist layer top (50% RH contour) lay between 900 hPa and 800 hPa. The weaker winds of this case implied lower Froude number flow for this case (Fr = 0.33) than the easterly wind case. Weaker orographic uplift and greater flow splitting than the easterly wind case at low levels was simulated for this case, likely a consequence of the lower Froude number flow. Weaker orographic uplift on upwind slopes led to less deepening of the moist layer on approach to W. Weak uplift combined with a shallow moist layer that didn't deepen significantly on approach to W led to no development of rain producing clouds over W. As well as these factors, strong wind shear across the moist layer top may have increased the entrainment of dry air from aloft. This entrainment hinders the development of cloud water droplets in the cloud top (Takahashi 1980).

Despite lacking in rainfall, W was still the point that had the most frequent cloud cover over the simulation. During the afternoon (e.g. Fig. 4-5) clouds developed over the southwestern side of the island possibly due to island heating and upslope flow. The deepest clouds formed over the southwestern low lying areas as clouds and light showers drifted ashore. A lack of orographic uplift and moisture over the mountains prevented these clouds from developing further as they moved inland. In northwestern low lying areas of the island, occasional afternoon clouds formed in upward moving air associated with the low level convergence of the sea breeze and down slope flow. Cloud over W formed mainly during the nighttime hours (e.g. Fig. 4-6) and was never more than a few

hundred meters deep. This suggests that this cloud was formed from radiational cooling of the mountain top surface and therefore could be considered a modeled mountain fog.

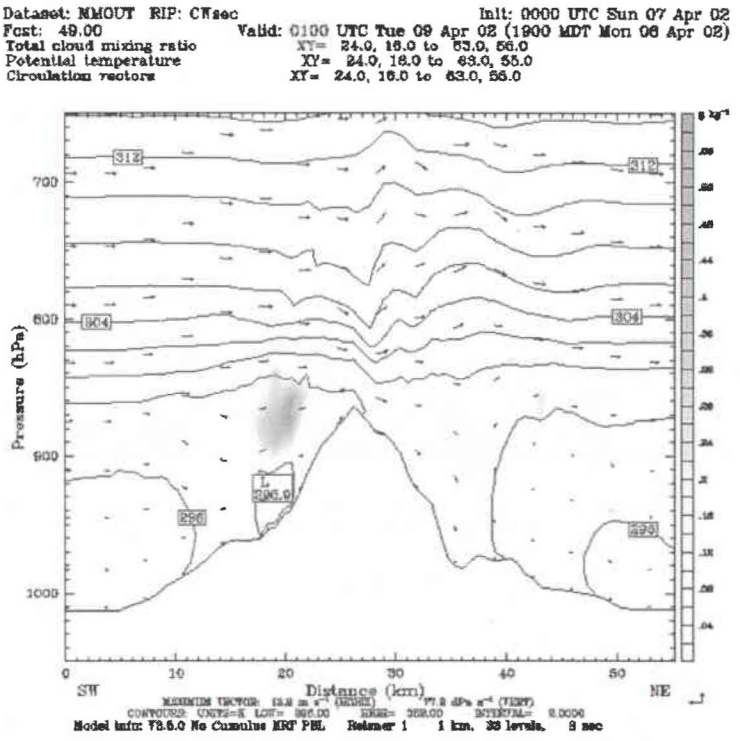

Figure 4-5: Cloud water (shades of grey in g kg^{-1}), potential temperature (contours in K) and wind vectors for the southwest northeast oriented cross section shown on Figure 3-8. The maximum vector in the horizontal is 13.9 m s^{-1} (if a horizontal vector component were to reach the beginning of the next then the horizontal wind speed would be 40 m s^{-1}) and in the vertical is 8 Pa s^{-1}) Plotted at hour 49 of the simulation (1500 HST on 8 April 2002), the same time as the surface wind plot of Figure 4-3.

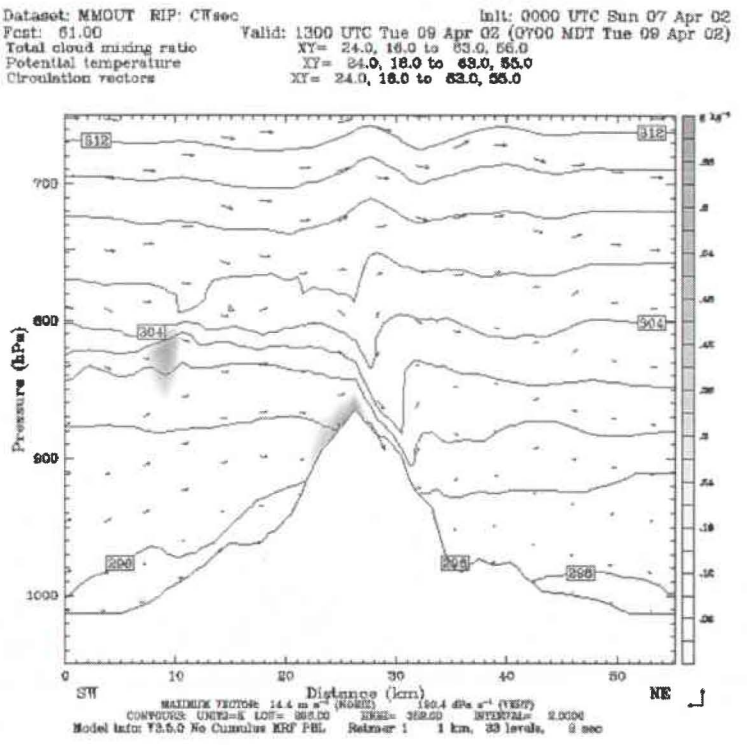

Figure 4-6: As Figure 4-5 but for hour 61 (0300 HST 9 April), the same time as the surface wind plot of Figure 4-4. Maximum vertical velocity vector is 12 Pa s^{-1}.

4.2 Case 3: Shear line of 24 to 27 January 2000

4.2.1 Background

This case covers a period when a weak shear line approached the Hawaiian Islands and passed over Kauai. A shear line is the trailing end of a cold front characterized as having only a weak temperature gradient across it. The wind direction usually changes from easterly ahead of the shear line to north easterly behind it. The shear line weakened through the simulation period and dissipated towards the end. Synoptic charts indicate that the shear line passed over the island around 0400 HST on 26 January 2000. Figure 4-7 indicates that an area of high pressure had developed to the west of the shear line, centered at 165°W, 33°N, by 0200 HST 26 January. This high migrated southeast and lay centered at 160°W, 27°N by 0800 HST on 27 January. A secondary low pressure system developed on the shear line trough as shown on Figure 4-7. This low developed further and moved towards the southeast so that at the end of the simulation it lay centered at 140°W, 30°N with an estimated central pressure of 1000 hPa.

The 300 hPa winds were westerly to north north-westerly over the islands throughout the simulation. By hour 43 (0300 HST 26 January) flow was more west northwesterly as an upper level trough lay to the northwest of Kauai. Figure 4-8 shows that the trough was passing over Kauai by hour 55 (1500 HST 26 January). By the end of the simulation the trough had passed over Kauai and the 300 hPa flow was north north-westerly.

An approximate open ocean wind speed of 10 m s^{-1} corresponds to Fr = 0.66 (given h=1500m and N = 0.01 s^{-1}) however this is even more approximate than for other cases because the open ocean conditions changed significantly as the case progressed.

Over Lihue the model soundings reveal that the period leading up to the shear line passage (the pre-shear line stage) was characterized by a strong trade wind inversion with a base at between 850 hPa and 750 hPa. As the shear line approached the inversion weakened and then disappeared as mid-tropospheric (between 700 hPa and 400 hPa) temperatures dropped. A weak inversion had formed at 850 hPa by the final hour after the shear line had passed. The K index was negative before and after the shearline passage averaging out at -2 for the entire simulation corresponding to a 0% chance of airmass thunderstorms. Hour 54 during the shearline passage had a K index of 33 which corresponds to a 60 to 80% chance of airmass thunderstorms.

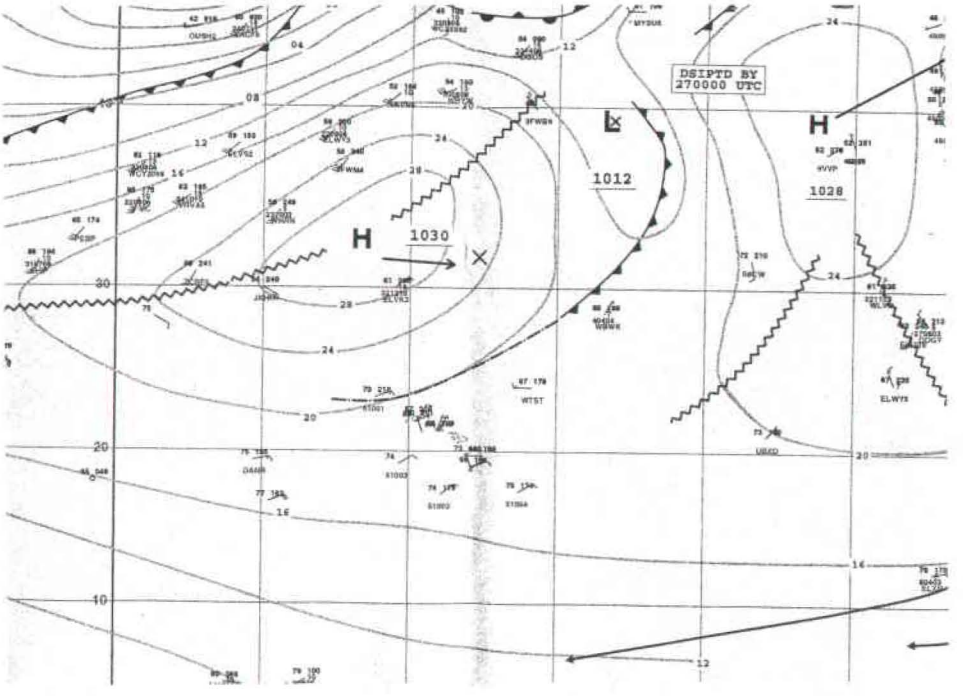

Figure 4-7: Surface pressure analysis for 1200 GMT January 26 (0200 HST, 26 January 2000).

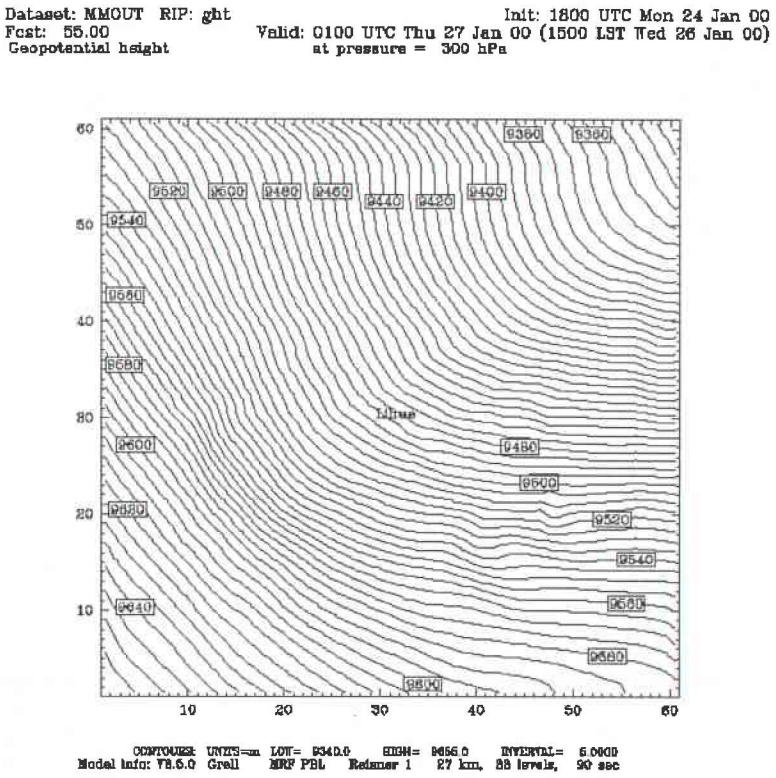

Figure 4-8: Model geopotential height at 300 hPa for domain 1 at 1500 HST on 26 January, contour interval is 5 meters

4.2.2 Rainfall

The island rainfall for this case fell almost entirely in the last 16 hours of the simulation during and after the shear line passage. I will present here a brief description of the rainfall during the last 16 hours of the simulation:

Hour 52-59: Rain occurs over the ocean to the north of Kauai and over north Kauai. This area of rain moves south over the island with smaller totals as it passes over the southern half of the island. Totals in the north Kauai are between 10 and 30 mm for this period.

Hours 59-61: Rain falls over northeast Kauai with a total rainfall maximum in the region of W. There is about 10 mm of rain across NW Kauai

By hour 61, 50 mm+ of rain has fallen over W in the past 10 hours.

Hour 62 shows a rain shower pass to the south of W producing totals of 30 mm over areas of the south coast in 1 hour. There is also significant rain on the southern slopes of W.

Hours 63-66 produced orographic rain that increased the Waialeale total to 60 mm for the entire simulation

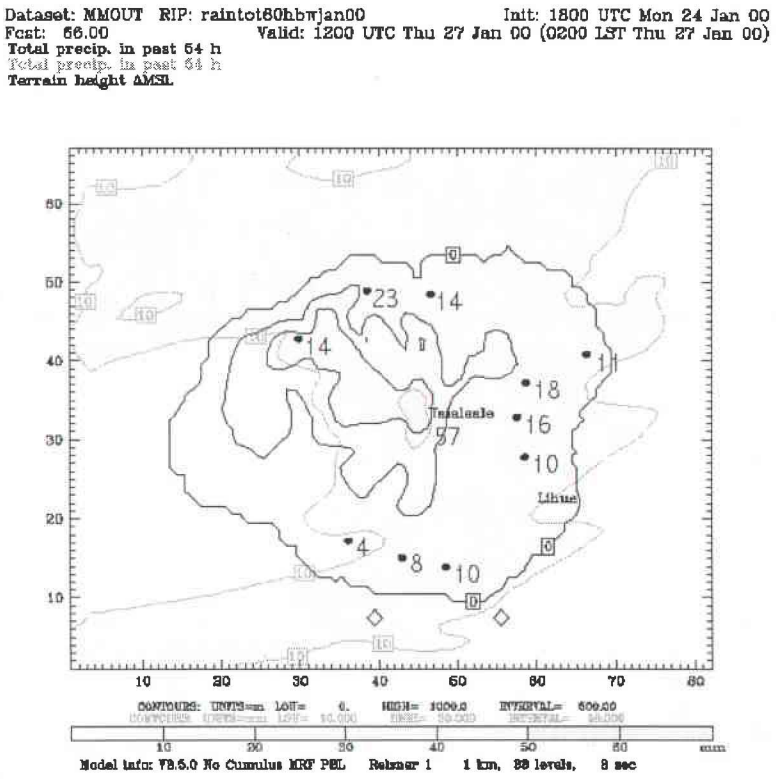

Figure 4-9: Total modeled rainfall in mm, excluding the first 12 hours, for the shear line simulation

Figure 4-9 shows that the total rainfall for the simulation produced a maximum over the central mountains. The first area of rainfall that passed over the island occurred after a deepening of the moist layer between hours 48 and 53. Rainfall fell over west Kauai and orographic enhancement of rainfall was not strong. Little rainfall fell over leeward areas suggesting that the presence of the upwind mountains had inhibited rainfall.

This case is of interest in terms of rainfall because it went through 3 distinct stages: 1) the pre-shear line stage, 2) the shear line passage, and 3) the post shear line stage. The pre-shear line stage appeared to have a diurnally pulsating shallow moist layer. The moist layer deepened during the afternoons of 24, 25 and 26 January and became generally shallower during the nighttime. The afternoon of 24 January however was during the spin up period of the model, and the afternoon deepening of the moist layer on the 26th was clearly related to the approach of the shear line and so it is unclear how significant this diurnal pulsation is. The thinning of the moist layer during the night of the 25-26 January produced the most dramatic example of leeside drying of any of the simulations. At 0000 HST on 26 January dry air from aloft had been advected down the leeside of the mountain from above the moist layer down to the southwest coast as shown in Figure 4-10. The shallow moist layer combined with down-slope flow enhanced by nocturnal down-slope (down valley) and land breeze flow, may be the responsible factors that forced this strong leeside down-slope advection of dry air from aloft. Whether the model is replicating a realistic feature of these conditions is highly uncertain and warrants further investigation using observations.

The passage of rainfall associated with the shear line crossing the island occurred during hours 52 to 54 (1200 to 1400 HST 26 January). This brought some rain for the entire island except for a small area of the southeast coast. After the shear line had passed the island was left in moderate northeasterly winds (about 10 m s^{-1}) and rainfall was confined mainly to the mountains, particularly W. It is this period that likely notched up W's total so that in the total rainfall it once again remains the wettest spot. As the shear line passed rain was not especially enhanced over the mountains, while after

the shear line had passed and the moist layer had thinned, rain continued over the mountains when the rest of the island was largely dry.

Precipitable water over the open ocean was 10 to 30 mm, 20 to 50 mm and 10 to 50 mm for the pre-shearline, shearline and post shearline stages respectively. Over Waialeale the precipitable water was 5 to 20 mm, 10 to 30 mm and 5 to 20 mm respectively. The variation in the depth of the moist layer over the different stages largely explains these variations.

This case highlights the importance of both wind speed and moist layer top elevation in producing large rainfall gradients across the island. The weak winds (5 m s^{-1}) and shallow moist layer of the pre shear line stage inhibited the development of rain producing clouds over the mountains. The passage of the shear line produced a deep moist layer and moderate winds (10m s^{-1}). Rain was widespread over northern areas with minimal enhancement over the mountains. There was less dry air advected down from above over lee areas. The transition from rising air to descending air over W was weaker than the easterly wind case consequently it is likely that this trigger of rainfall was not focusing rainfall over the highest ridges as markedly. The lack of a trade wind inversion near the mountain top may have inhibited the development of down-slope winds therefore weakening the fallout of rainfall over W. After this deep moist layer had passed the moderate winds of 10-15 m s^{-1} coupled with a lowering of the moist layer top, returned the rainfall distribution to one more similar to that of the easterly wind case. The presence of the moist layer top (and trade wind inversion) at an elevation above, but not too far above (approximately 50-150 hPa above), the mountain top appears to be one key condition that focuses rainfall over Mt Waialeale (discussed in section 3.5).

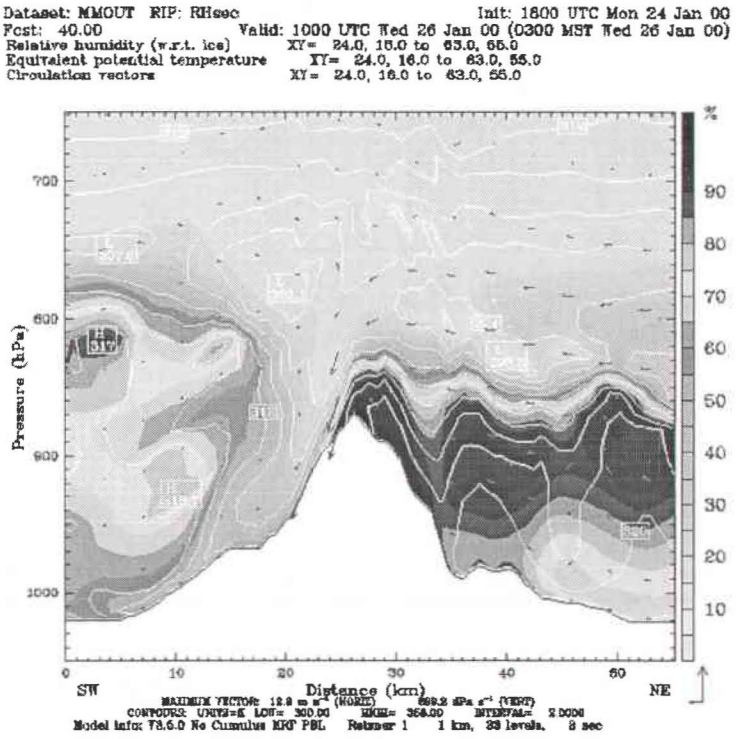

Figure 4-10: South west to north east oriented cross section (as in Figure 4-5) showing relative humidity (colors, %), equivalent potential temperature (white contours in K) and wind vectors for hour 40 (0000 HST 26 January 2000). Maximum vertical velocity vector magnitude is 30 Pa s^{-1} (this occurs in the down-slope flow just to the lee of W).

4.3 Case 4: Wintertime strong northeasterly flow of 18 to 21 January 2002

4.3.1 Background:

This case covers a period when there was a strong subtropical high to the northeast of the islands. Throughout the simulation the high pressure system had a central pressure of approximately 1040 hPa +/-5 hPa. The high was initially centered at 140°W, 40°N and then throughout the simulation it moved gradually towards the southwest. At the end of the simulation the high lay stationary north of the islands centered at 157°W, 37°N. This intense high set up a strong pressure gradient over the Hawaiian Islands (shown on Figure 4-11) leading to strong northeasterly winds throughout this period.

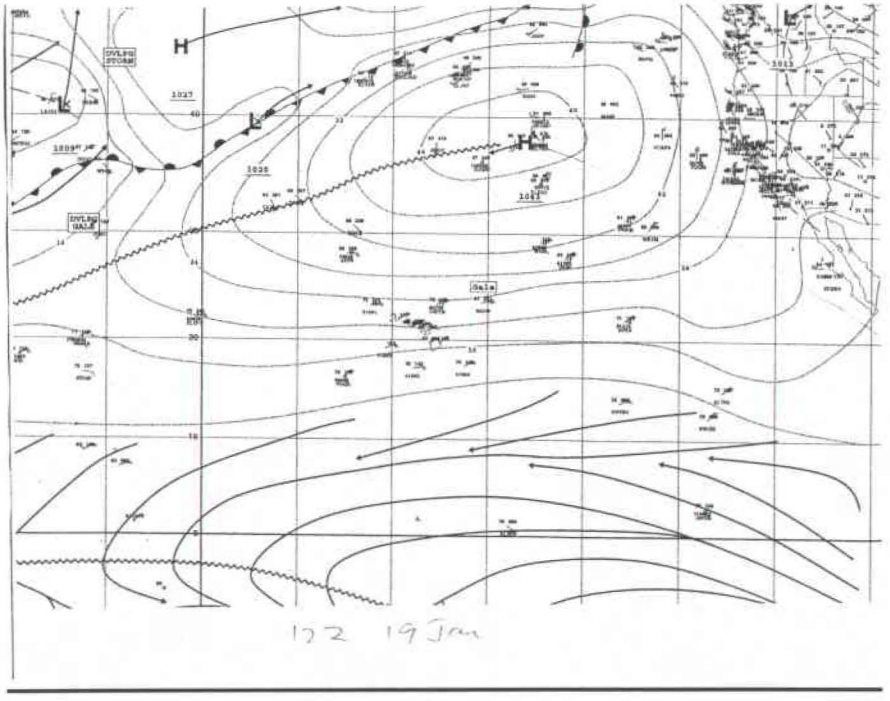

Figure 4-11: Surface pressure analysis for 1200 GMT (0200 HST) 19 January 2002.

At upper levels a deep upper level low developed to the northeast of the islands and migrated southwards towards and over the Big Island. The modeled 400 hPa winds for 0200 HST 19 January are shown on Figure 4-12. Cold temperatures and predicted heavy snowfall warranted the issuance of a winter storm warning for areas above 7000 feet of the Big Island and Maui.

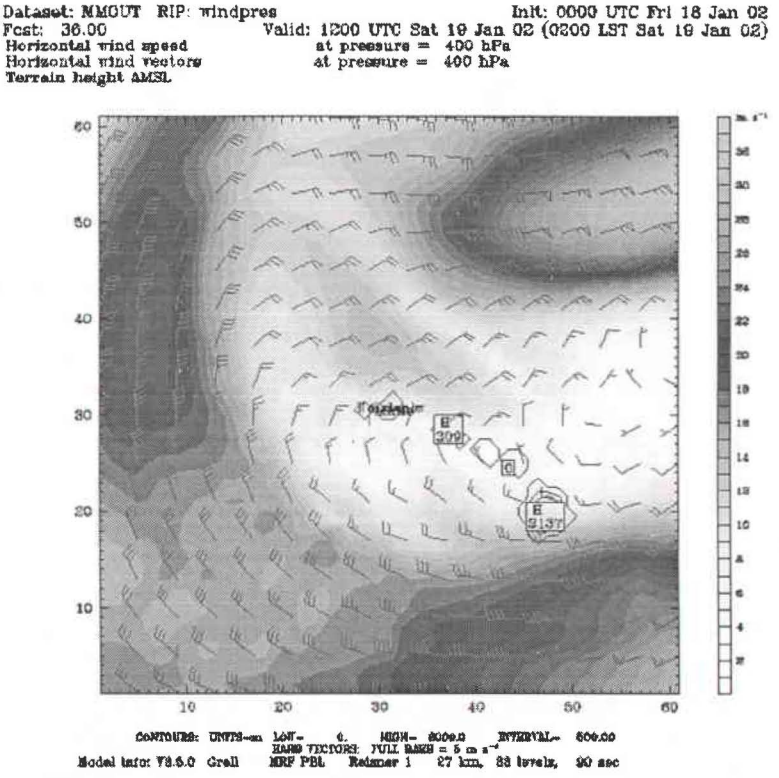

Figure 4-12 Wind speeds (shades m s^{-1}) and directions (barbs: one full barb is 5 m s^{-1}) at 400 hPa for hour 36 (0200 HST 19 January 2002)

As well as the winter storm warning, a heavy rain warning was issued for Hilo and Puna on the 18 January. A high wind warning was issued on 18 January for the Big Island and Maui with 35 to 45 mph winds forecast and gusts of 60 mph. A heavy rain warning was issued for northeast Maui (Hana road) on 20 January and a high surf

warning was issued for east coasts on the 20 January due to 8 to 12 feet (face) waves that had been generated by the strong northeasterly winds.

At 400 hPa winds were initially west northwesterly but shifted to being northerly for the majority of the simulation as the upper level trough remained to the east of Kauai. This northerly flow cooled mid levels, weakening the TWI and destabilizing the airmass. Over Lihue the trade wind inversion base was present at 800 hPa at hour 12 of the simulation (the first hour considered for analysis) however for the remainder of the simulation it was either absent or weaker and at 700 hPa or higher. Modeled CAPE reached a maximum of 466 J kg^{-1} at hour 18 but was zero for the majority of the simulation. Again the model seemed to underestimate CAPE over Lihue as observed CAPE was between 174 and 1462 J kg^{-1} for the 12 hourly observational soundings. The average K index for the model soundings was 23 corresponding to a 20 to 40% chance of airmass thunderstorms.

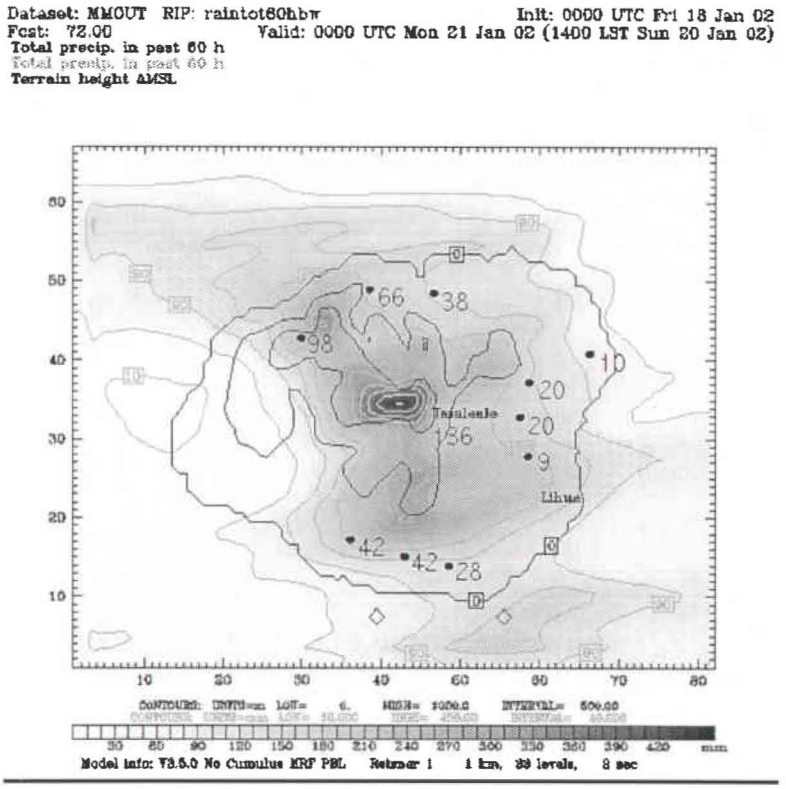

Figure 4-13: Total 60 hour rainfall (mm) excluding the first 12 hours of the strong northeasterly wind case.

4.3.2 Rainfall

This case produced the largest modeled rainfall totals over the island of all the cases. Rainfall generation over W was very consistent as for almost every simulation hour some rain fell at this location. Many heavy showers fell over the island and they were strongly enhanced over the mountains. As a consequence the total rainfall for the case once again has a very strong orographic signature (Fig. 4-13). This suggests that orographic forcing was rapidly triggering the development and fallout of rain over the mountain areas. Despite the very heavy rain over the mountains throughout this simulation there was less than 10 mm over an area of the west coast implying that showers were strongly suppressed over this area.

Over W some 450 mm of rain was modeled. This compares very poorly with the observed total of 136 mm at the Waialeale rain gauge for this period. Other stations also recorded much less rainfall than the model simulated. It is possible that some of these large discrepancies could be due to problems of rain gauge rainfall measurements in periods of strong winds. Perhaps more likely than (or as well as) this is the possibility that the model did a particularly bad job at simulating this case. This problem will be discussed further in section 6.1.

This case had a highly variable moist layer and also at times shallow layers of humid air at higher elevations, as on Figure 4-14. The passage of frequent deep clouds occurred particularly in the latter half of the simulation. As the clouds passed over W they often decayed, fragmented or dissipated as descending air on the lee side pushed dryer air downwards, and inhibited convection. In this simulation the moist layer was often deeper above the lee side of the island although the average RH within the moist layer was lower on the lee side because of the downward advection of dry air. The residue of the convection that developed on the windward side combined with vertical mixing on the lee side could be responsible for the upward transport of moisture as air passes over the island. The Fr for this case was high (again assuming $N = 0.01\ s^{-1}$ and h = 1500 m), roughly = 1 because of the variable strong winds (10 to 20 m s^{-1}) leading to strong flow over the island and leaving little opportunity for diurnal thermal circulations to show any clear signal.

Precipitable water was 20 to 60 mm over the open ocean and 10 to 35 mm over W. In specific cells precipitable water was larger reaching a maximum of 80 mm over the Lihue Basin at hour 26 (1600 HST on 18 January). As for case 1 this reduction in

precipitable water between the ocean and W is due to a combination of rainout and moisture divergence.

Despite the highly variable rainfall and variably deep moist layer of this case the total rainfall produced very large gradients in rainfall across the island. For example from W to the West coast there was a rainfall gradient of 12.4 mm km^{-1}. The strong winds of this case appear to be a key factor that enabled this large gradient to develop because they force high Fr No, flow that leads to a strong vertical motion transition over W.

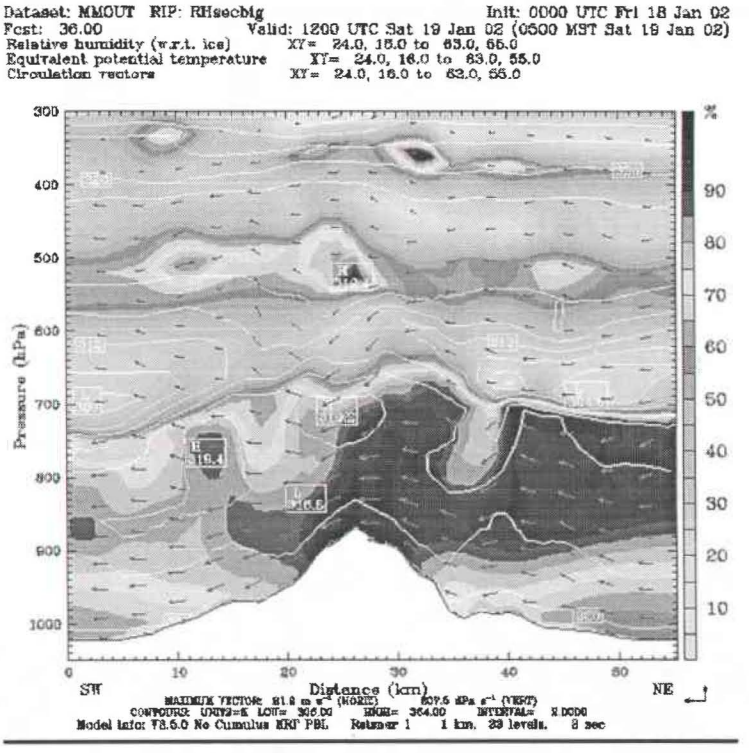

Figure 4-14: Relative humidity (colors in %) theta-e (contours in K) and wind vectors (arrows) for a SW to NW cross section across Kauai for hour 36 (0200 HST 19 January 2002) of the strong northeasterly wind simulation. This cross section is thicker (1000 hPa – 300 hPa) than those of the previously discussed simulations. Maximum vertical velocity vector component is 21 Pa s^{-1}.

4.4 Case 5: Kona Storm of 2 to 5 November 1995

4.4.1 Background to case:

This case covers a period when a kona low developed to the northwest of the Hawaiian Islands shown on Figure 4-15. Moist low level southerly flow and unstable air to the southeast of the low produced deep convection near Kauai on the 2-4 November 1995. An observationally based analysis of this case is presented in Businger et. al (1998), and a modeling analysis using the Regional Spectral Model (RSM) is included in Wang et. al. (1998).

Kauai lay to the southeast of the kona low and lay in convective southerly flow that triggered many deep showers and thunderstorms. Winds were variable southerly to southeasterly of between 3 and 10 m s^{-1} over the upwind ocean at the surface with more southwesterly winds above 700 hPa. This corresponds to an approximate Fr of between 0.2 and 0.66. Fr was therefore lower than the easterly wind case and diurnal circulations did develop in the surface wind flow although they were not as clear as for the weak SW wind case probably because of the variable wind and the passage of convective cells.

Modeled CAPE was high over Lihue for the 6 hourly soundings, averaging 767 J kg^{-1} over the 60 hours analyzed and reaching 1496 J kg^{-1} at hour 24. The observed sounding at hour 12 (0000 GMT on 3 November) showed CAPE = 2022 J kg^{-1}. After this sounding the next radiosonde launch was at hour 60 (0000 GMT on 6 November). The launch site had been struck by lightning according to Businger et al. (1998) and consequently five crucial launches were missed during the event. The average K index for this case was 30 corresponding to a 40 to 80% chance of air mass thunderstorms.

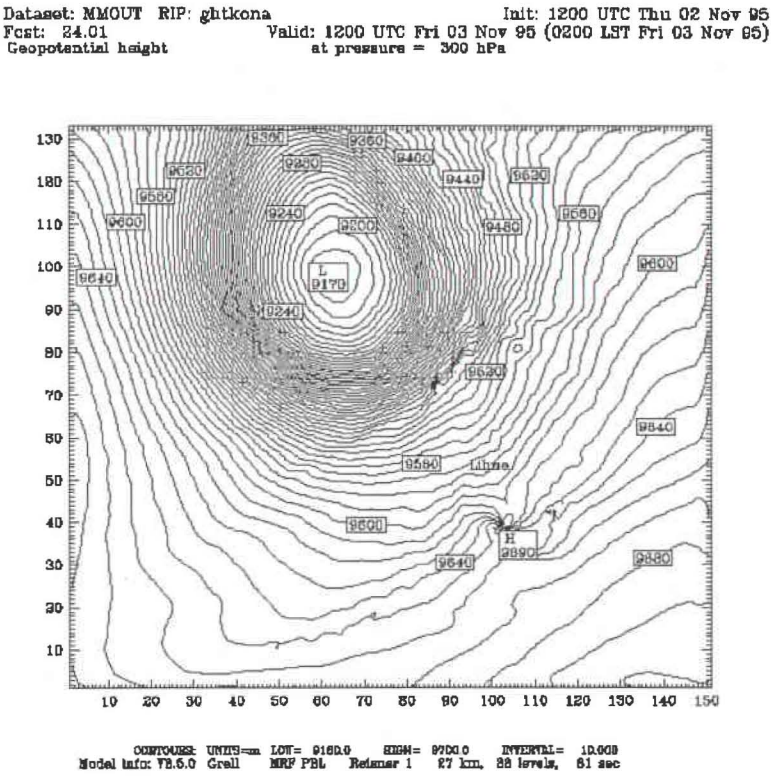

Figure 4-15: Modeled geopotential height (m) at 300 hPa for 0200 HST 3 November 1995. Contours are every 5 m.

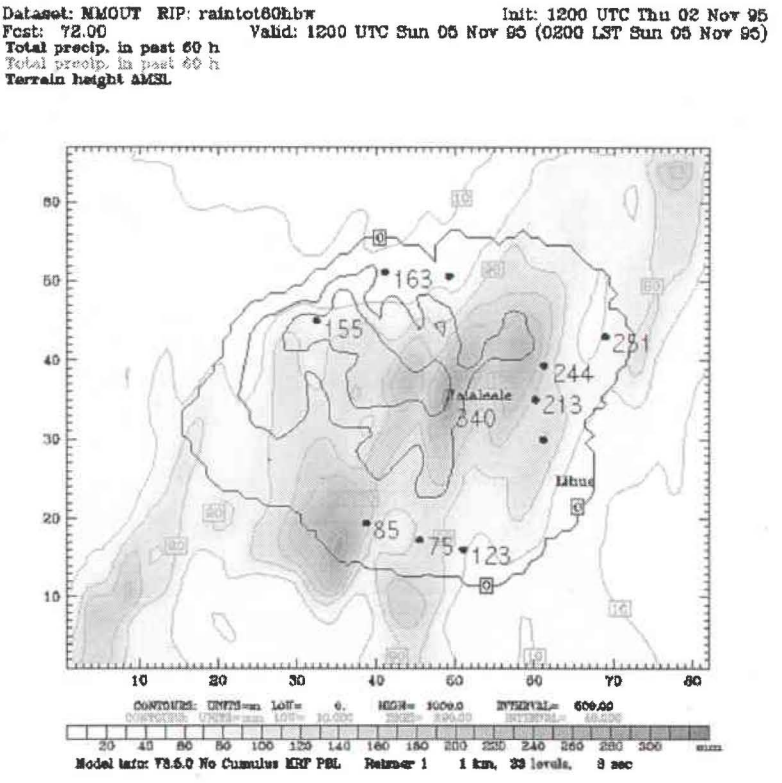

Figure 4-16: 60 hour total rainfall (mm), excluding the first 12 hours of the simulation, for the 1995 kona low case.

4.4.2 Rainfall

Over the course of this case the model produced many heavy convective showers over the island. Consequently the rainfall totals are highly variable across the island, as shown in Figure 4-16. The highest totals are just east of W and over a small region of the southwest coast where over 300 mm was modeled. Two very heavy localized convective rainfall events towards the end of the simulation were largely responsible for the maximum over the southwest coast. This case is interesting as it produces significant rainfall over the usually dry southwest coast as would be expected for an event like this. Rainfall was far less orographically dependent than it was in the easterly wind case although it is still apparent that orographic forcing produced more rain over the mountains than over most of the lower island areas.

The case produced numerous outbreaks of deep convection triggered by orographic uplift. In general uplift of air to its level of free convection over the mountains would have triggered moist convection in the conditionally unstable air. At times the convective cloud tops were higher than 300 hPa and produced more rain over the central mountains than over most coastal regions. However the heaviest showers of the simulation (up to 120 mm h^{-1}) occurred over the south coast in the hours leading up to 51 and 52 (0500 and 0600 HST on 4 December), and leading up to hours 69, 70, 71 and 72 (2300, 0000, 0100 and 0200 HST on 4 to 5 December). The surface wind fields suggest that convergence between the nocturnal offshore flow and the open ocean SE winds aided the development of these storms.

Precipitable water was approximately 40 to 70 mm over the open ocean increasing to 110 mm in individual convective events. Over W there was 10 to 50 mm of precipitable water. The deep moist layer of this case is responsible for the high precipitable water amounts. The largest totals occurred in regions of deep convection where moisture had spread throughout the troposphere.

This case stands out against the other cases with significant rainfall. The rainfall distribution over Kauai was less consistent with the annual rainfall (Figure 1-2) than the distributions for the other cases with significant rainfall (cases 1, 3, and 4). Nonetheless the maximum rainfall is still near W. Over the course of the simulation convection and associated rainfall was frequently generated over the mountains. This convection was most frequent over or just to the east of W. Air ascending up the steep eastern escarpment may be one trigger for these particular convective showers. The weak winds of this case may not have forced strong orographic uplift, however because of the

unstable conditions only weak uplift was required to trigger deep convective showers. It might be expected that daytime heating over the island would increased the CAPE during the afternoon and perhaps generated sea-breeze flows that converged over the island. Though these factors were probably important in the generation of convection the results did not show clear examples of afternoon convection triggered by daytime island heating.

This case shows a kona storm situation that triggered heavy leeward rainfall. Up to 300 mm of rain fell locally over some areas of the south coast that receive only 750 mm annually. This case therefore gives an indication of how a substantial proportion of annual leeward rainfall could be attributed to just a few wintertime kona storms.

5 Sensitivity of rainfall to model vegetation

5.1 Background

The most compelling evidence for vegetative feedbacks on climate is at the larger continental scales. For example the effects of the Amazon Rainforest on regional and global climate have been studied in Nobre et al. (1991) and Sud et al. (1996). These studies have shown that when the Amazon Rainforest is replaced by savanna in mesoscale and global climate models, there is a significant drying of the South American continental interior as well as other regional and global climate changes. The implied enhanced rainfall when rainforests are present is concluded to be a consequence of water recycling between the atmosphere and the forests and soil.

In addition to these large scale studies research has been conducted covering smaller scales more relevant to the scales dealt with in this current study. Blythe et al. (1994) did a mesoscale modeling study over southwest France during a frontal passage. They did simulations with observed forest and with forest replace by bare soil, in the model. The model showed a 30% increase in rainfall over the region when the forests were present. Two mechanisms for this increase in rainfall were stated: 1) Intercepted water re-evaporated from the forested areas, and 2) High roughness length of the forest leading to enhanced moisture convergence. The wet canopy low radiation (cloud covered) evaporation values were only possible by maintaining a negative sensible heat flux over the forest. The mechanism for maintaining this flux was concluded to be strong wind shear within a stably stratified boundary layer. These conditions are associated with a moist surface with high surface roughness such as a forest. The lower limit for the

horizontal scale of the forest required to initiate these processes was estimated as being 10 to 20 km. This lower limit was drawn in part from the 10 km grid resolution of the model.

There is some background of non-scientific evidence that vegetation on tropical islands could influence the local weather significantly. In the Caribbean as in Hawaii there has been considerable vegetation change since the arrival of western cultures. Bridenbaugh and Bridenbaugh (1972) tell of the introduction of sugar cane to St Kitts and other islands by the English colonists. There followed rapid deforestation and a possible reduction in rainfall. "The belief that forests attract rain is still widespread in the folklore of the West Indies" states Anthes (1984). Today there is significant rainfall variation between different islands. Topographic effects and island size can largely explain this variability; however, there is also some possible correlation with vegetation type.

In Hawaii local people have claimed that a cloud called the Makena cloud, which spreads from the slopes of Haleakala over towards the island of Kahoolawe, used to be more extensive and led to more rain over Kahoolawe (personal communication Prof. Thomas Schroeder and Prof. Tom Giambellucca). This cloud is said to have reduced in extent since the cloud forests of the upper slopes of Haleakala were replaced by ranchland. Is it possible that mountain forests on this kind of scale can play a crucial role in such a prominent meteorological phenomenon? Also in some Leeward areas of Oahu locals have said that deforestation has caused rainfall to go down (personal communication Prof. Tom Giambellucca and Prof. Thomas Schroeder).

It should be noted that there are many possible errors associated with these observations. Observed changes in island climate could be a consequence of climate

change or long period large-scale climate oscillations. Another possible source of error is in the fact that when forests are present, it is moister and cooler below the canopy than when there is only grassland. This may lead local people to the false observation that rainfall has gone down when in fact only the near surface has dried up.

One of the issues in Hawaiian meteorology is the debate between thermodynamic and dynamical processes as mechanisms in producing the observed weather features of the islands. Smolarkiewicz et al. (1988) states the case that features of the Hawaiian weather, such as the cloud band that often forms upwind of the Big Island can be explained by dynamical interactions between the trade wind flow and the island barrier. The thermodynamic argument e.g. Chen and Wang (1994) is that thermodynamic forcing also plays an important role in Hawaiian weather features. Chen and Wang (1994) concluded that diurnal fluctuations such as the upslope and down slope winds on the windward side of the Big Island result as a consequence of the diurnal evolution of the surface thermodynamic fields. These surface thermodynamic fields are dependent in part on the vegetation cover (Xue et al. (1990)) and so changes in vegetation may play an important role in the observed diurnal variations in surface conditions (temperature, humidity, and winds) on the islands.

Sensitivity to model vegetation sensitivity tests were performed on two of the case studies; the easterly wind case and the strong northeasterly wind case. For all of these simulations the vegetation was homogenous across the island. The soil type and the initial soil moisture was the same as the standard setup (see Chapter 2) for all of these simulations. For the easterly wind case of Chapter 3, the simulation was run with evergreen broadleaf forest, mixed forest, and sparse vegetation over the island. The

vegetation types are taken from the 25 category USGS dataset definitions. For the three vegetation types used, the physical parameters for northern hemisphere winter are shown in Table 2. For the strong northeasterly wind case of section 8 the simulation was run twice, first with mixed forest and secondly with sparse vegetation. The total rainfall for these sensitivity case studies was then plotted and compared to see if the vegetation changes had altered the modeled rainfall amounts and distribution over the island

Vegetation Description	Albedo (%)	Moisture Availability (%)	Emissivity (% at 9 μm)	Roughness Length (cm)	Thermal Inertia ($cal cm^{-2} k^{-1} s^{-\frac{1}{2}}$)
Evergreen Broadleaf	12	50	95	50	0.05
Mixed Forest	14	60	94	50	0.06
Sparse Vegetation	25	5	85	10	0.02

Table 2: Description and physical parameters for the three vegetation categories types selected for the sensitivity simulations of this section. These are taken from the 25 category (USGS) vegetation dataset for the northern hemisphere winter. (MMM NCAR 2000)

5.2 Results

60 hour rainfall totals for the five sensitivity case studies are shown on Figures 5-1 (easterly wind case) and 5-2 (strong northeasterly winds). For the easterly wind case there are some clear differences in total rainfall distribution for the different vegetation types but orographic forcing of rainfall retains a clear signal throughout the three simulations. W remains the focus of the largest rainfall totals with 150 mm, 150 mm, and 160 mm in the evergreen broadleaf, mixed forest, and sparse vegetation simulations respectively. These similar totals are not representative of the rest of the island where totals differed considerably. Over the northern ridges and valleys there was 20-30 mm less rain for the sparse vegetation case when compared with the two forested cases that

had similar totals in this region. The prominent ridge extending south from W had similar totals for the three case studies at around 50 mm. A prominent maximum in rainfall occurred over the lower elevations near the south coast for the sparse vegetation case with a maximum of 70 mm of rain. This compares with 40 mm and 30 mm in this region for the mixed forest and evergreen broadleaf cases respectively. In general although the sparse vegetation case has the largest total over W, it is the evergreen broadleaf simulation that appears to focus the orographic rainfall over the central mountains and valleys of the island.

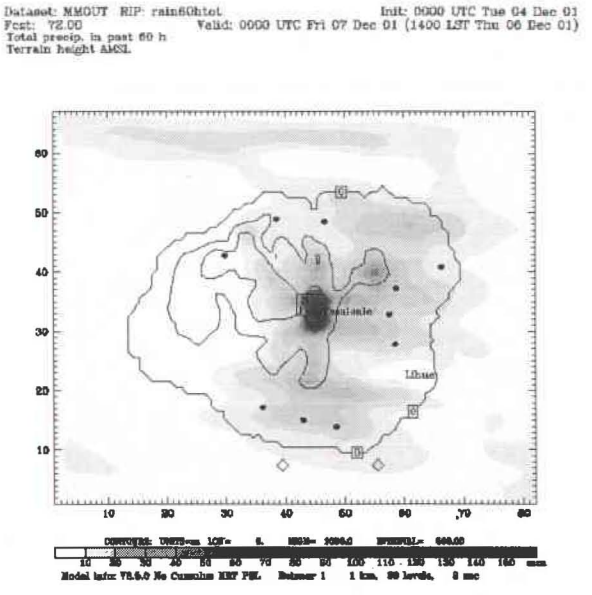

a)

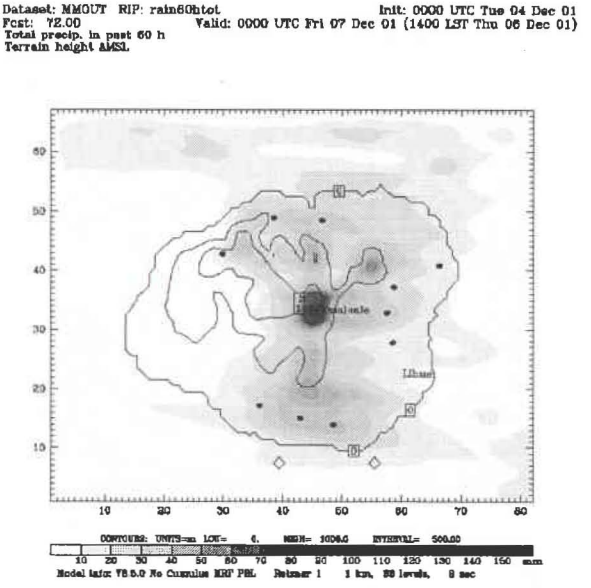

b)

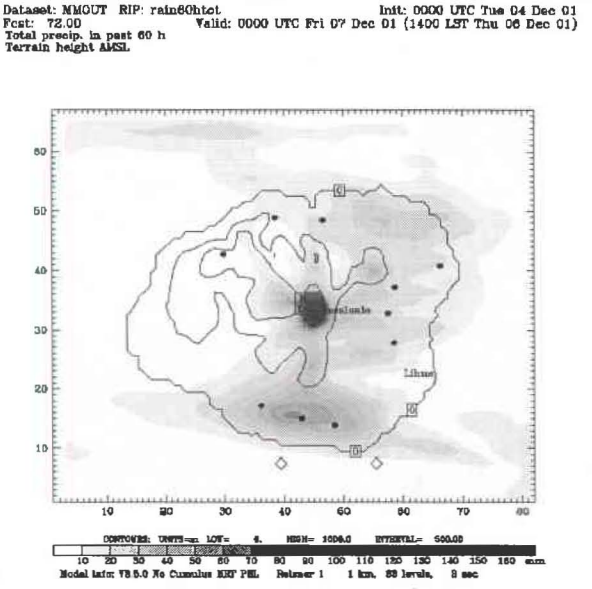

c)

Figure 5-1: Total 60 hour rainfall for the easterly trade wind case for a) evergreen broadleaf forest b) mixed forest and c) sparse vegetation.

For the strong northeasterly wind case there were also differences in model rainfall for different vegetation types. For the mixed forest case there was more rainfall over W and over the mountains to the south as shown in Figure 5-2. Rainfall was also greater over the sea upwind of much of the east coast for the mixed forest case suggesting

that the larger rainfall totals over W may be due primarily to differences in the upwind forecast rather than to local differences in the vegetation.

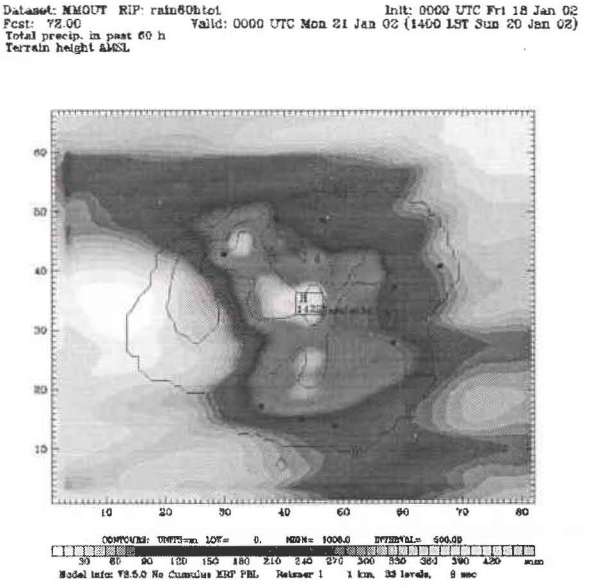

a)

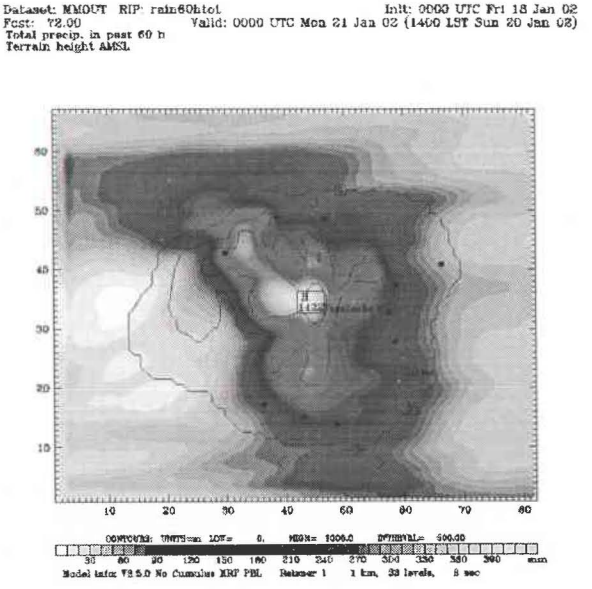

b)

Figure 5-2: 60 hour total rainfall for the strong northeasterly wind case for a) mixed forest and b) sparse vegetation.

5.3 Discussion of vegetation sensitivity case studies:

The sensitivity tests here show that changing the vegetation type in the model changes the rainfall distribution over the island for these two case studies. Each of these simulations presents a different forecast because of the change made to the vegetation and the consequent almost chaotic consequences of that change. The predictability of individual clouds and cloud systems will vary between the simulations, even upwind of the island, therefore establishing whether vegetation was the key cause of the simulated changes in rainfall between the cases, is difficult.

The Easterly wind simulation could be showing some significant effects of model vegetation on rainfall production over the island. The sparse vegetation simulation shows less rainfall over the northern mountains and valleys for this case yet has more rainfall over Waialeale than the other two cases. It is plausible that these changes in rainfall distribution are a direct consequence of changing the vegetation type in the model. The changes to the surface fluxes of heat and moisture could influence the development of rainfall over the island. As an example the forested vegetation is parameterized in the model as having enhanced moisture availability and roughness length than the sparse vegetation, as shown in Table 2. Enhanced moisture availability at the surface reduces the dew point depression in this near surface air. The lifting condensation level of this surface air will be lowered for this air. Therefore if this air is forced up the mountain slopes, clouds may develop at slightly lower elevations. According to Takahashi (1981) a lowering of cloud base enhances the development of cloud droplets because the onset of cloud droplet growth is at lower elevations and the cloud produced is likely to be deeper. These changes to cloud development under trade wind conditions may be enhancing the

development of rainfall in certain areas and retard it in others. Changes to surface temperature and dew point temperature over different surface types are likely to also affect the stability and buoyancy of the near surface air. Surface temperature changes affect the convective available potential energy (CAPE) of the atmosphere over the island. Under light wind conditions, in particular, vegetation and soil properties will influence the development of convective clouds as well as land and sea breezes and associated areas of convergence.

Why is it of interest to perform further sensitivity tests to vegetation and soil properties over the Hawaiian Islands? If vegetation physically influences rainfall under trade wind conditions, it will affect the distribution of average rainfall across the island. This will in turn modify the growth of plant species across the island, with time. Over large periods of time, the growth, spread and competition of different plant species could tend for plants that thrive best in wet conditions to enhance the rainfall over that region. Forests that tend to enhance downwind rainfall (say, in a valley on the lee side of a ridge) may tend to spread into that valley region; i.e. the forests on the upwind slopes and ridges will affect the microclimate of the valley downwind. The Hawaiian Islands may provide a particularly good example of these kinds of vegetation-induced microclimatic influences because of the consistency of the trade wind climate. With improving numerical models tests of these concepts will become more accurate. These possibilities provide sufficient reason for continued investigation into the effects of landscape properties on Hawaiian weather.

6 Discussion and Conclusion:

This study has use real cases to model the weather over the island of Kauai using MM5. The model simulates realistic orographic rainfall over the island for 4 of the 5 cases when compared to rainfall observations. The easterly wind case models an example of the most common trade wind flow over the island. The individual hourly rainfall did not match observations; however, the total rain over the period agreed well, particularly the island wide distribution. This suggests that the model is successfully modeling the development of trade wind orographic cloud and rain over the island over time periods of days. The model is incapable of reproducing each individual rainfall event but over longer time periods the distribution of rainfall correlates with observations due to correct production of showers over particular areas (e.g. over the mountains). The similarity between the total rainfall pattern for the case (Fig. 3-6), the pattern of the annual rainfall (Fig. 1-2) and the rainfall of individual summer months (e.g. Fig. 1-4) suggests further that the model is simulating the island wide rainfall distribution realistically. The model simulates for 60 hours of easterly wind flow approximately 10 times more rain over the Mount Waialeale region than over the upwind (east) coast. Approximately 10 times more rain is also observed annually between the coast and Waialeale. The similarity can also be interpreted as a sign of the dominance of trade wind rainfall in determining the island wide rainfall distribution over monthly and yearly timescales.

The shear line case modeled the passing of a weak shear line over the island. The wind direction was out of the northeast for the entire simulation but the wind speed increased as the clouds and rain associated with the shear line passed over the island.

The wind direction led to a rainfall distribution similar to that of the strong northeasterly case; however, the island-wide gradients in rainfall were less for the shear line case.

Both of these cases show significant offshore rainfall to the northwest and to the south of the island. This is likely a dynamic effect of the flow over and around the island topography triggering offshore showers. The fact that this offshore rainfall pattern is most pronounced over the periods of strongest winds (as the shear line passed, and for the entire strong northeasterly wind simulation with open ocean wind speeds of around 15m s^{-1} or greater) may suggest it occurs as a consequence in part of high Froude number flow over the island. Rainfall near the edge of the domain may also be affected by the domain boundary. It has been observed in this study that the transition of air across nest boundaries has an effect on wind and rainfall pattern that sometimes appears unrealistic (see below).

6.1 Problems:

It is difficult to know how realistic these simulations are compared to reality. The nesting technique leads to some unrealistic features. The most obvious one is an abnormal region of strong winds that originates out of the upwind corner of a domain at certain times. This was mentioned in section 4.1.2 for the weak southwesterly wind case. These strong corner jets (as I call them) can spread across the 1 km domain seriously influencing the flow over the island and consequently cloud and rain. They are clearly an unrealistic numerical artifact but I do not know their cause.

One of the key features that should be modeled correctly for Hawaii is the trade wind layer. This layer usually consists of many shallow clouds that force convection and mixing at small horizontal and vertical scales. Although the easterly wind case appeared

to simulate good trade wind orographic rainfall it is unclear how accurately the small scale open ocean structure of the trade wind layer is being simulated at the horizontal and vertical scales of the model. The model relies entirely on the explicit microphysics scheme for simulation of trade-wind clouds at the 3 km and 1 km resolution domains. If the simulation of trade wind clouds is unrealistic then the modeled vertical mixing of moisture and consequently the moist layer structure may also have problems. Since observed trade cumuli have typical volumes of 1-10 km^3, it would be surprising if these clouds were accurately simulated.

6.2 Discussion of key questions:

With reference to the model results a number of key questions are discussed in this section.

Why is there persistent cloud over Mount Waialeale?

For typical trade wind conditions (for example a moist layer top at 2000 m and an open ocean wind speed of 10 m s^{-1}) Kauai's shape and the elevation of Mt Waialeale enable air to be lifted up from lower levels over the top of the mountain. This lower level air arrives from the open ocean, unaffected by any significant landmass, where sea surface temperatures do not vary greatly with the seasons. This maritime air tends to have a dew point depression that when lifted up windward slopes correspond to a lifting condensation level of between 600 m and 1500 m. Clouds will therefore form on the windward side of Waialeale (1569 m) if near-surface air flows over the summit. Typically Mt Waialeale lies below the open ocean moist layer top (the trade wind inversion, TWI), often between 1500 m and 3000 m. Also the flow of air over the

mountain tends to raise the moist layer top over the mountain, thus enabling a layer of very humid air to exist over the mountain even perhaps when the TWI height upwind is close to the mountain's elevation. The latent heat generated by cloud formation on windward slopes further aids flow over the mountain by increasing the buoyancy of the air.

Under conditions of weak winds, fog may form over the mountains caused by nocturnal cooling of the mountain surface to the air's dew point. Daytime generated convection anchored over the mountains, associated with island heating. The generation of a sea breeze and daytime valley flows may also aid upslope flow to the LCL, hence generating clouds over the mountains. Cloud free periods may be associated with light winds and a shallow moist layer when there is weak upslope motion and the air over the summit is relatively dry.

Why is there 10-15 times more rainfall annually over Mt Waialeale than over the open ocean and windward coasts?

Rainfall over Hawaii is dominated by trade wind rainfall. The easterly wind case showed similar gradients of rainfall across the island to those observed. Upward moving air and the raising of the moist layer top, lead to a general deepening of existing clouds (and the formation of new clouds) between the windward coast and the central mountains. Deepening clouds will aid the development of cloud water and rain droplets and this may account for the increase in rainfall observed over windward areas. Over the summit of Waialeale the moist layer depth is usually shallower than over the windward slopes a few kilometers upwind. It is likely that the air flow transition from up windward slopes to down lee slopes is crucial in triggering the heavy persistent rain over the

summit. This follows the observations of trade-wind clouds in Takahashi (1981) and the concept of a "mini cloud burst" over Waialeale described in Ramage and Schroeder (1999). The halting of upward motion and commencement of downward motion over the summit crest of the island should trigger the fall out of large numbers of cloud and rain droplets. These falling droplets will grow further through coalescence with other droplets. Downward moving air not only forces the removal of moisture through rainfall but also entrains dry air from aloft into the moist layer below. Clouds are therefore likely to become smaller or dissipate over lee slopes; however over upper lee slopes there may be frequent cloud cover but usually only small cloud droplets or drizzle as the heavier, larger droplets would have fallen out over the summit crest or windward side.

The dependence of orographic cloud and rain on the transition in air vertical motion over the mountains is in turn dependent on the factors forcing the air flow over the island. Some of these factors include i) The low level wind strength, direction and vertical shear, ii) The stability and buoyancy of the low level air, in particular the strength and height of the TWI and the depth of the moist layer, iii) large scale upper and lower tropospheric forcing, and iv) the presence or absence of upwind clouds.

The presence of a temperature inversion not far above the mountain top will strongly affect the flow over the mountains. Durran (1986) showed that the production of a strong down-slope wind event was dependent on the presence of a temperature inversion in the case of a Boulder, CO windstorm. It was suggested that an amplification of the surface wind occurred as a low-level inversion was displaced downward along the lee slope, producing a supercritical flow. Since the flow along the lee slope is supercritical it should continue to accelerate eventually recovering to the ambient downstream

conditions in a turbulent hydraulic jump. The presence of the TWI may in turn tend to increase the gradient in rainfall down lee slopes as stronger down-slope winds will enhance cloud dissipation. The enhanced transition between upslope and down-slope motion associated with the TWI over the summit crest could also boost the fallout of rain over the summit crest. Thus the presence of the TWI a short distance above the mountain top is likely to be a key factor in producing the huge gradients in rainfall across the island, especially down the lee slopes.

Finally another important factor in the forcing of downward motion over lee slopes could be lifting of unsaturated air, combined with evaporative cooling near the inversion level above the summit crest. Hall (1980) showed the evolution of a warm rain maritime cloud using a detailed microphysical cloud model. His results showed that when the cloud was developing, a "cold dome" of air formed above the cloud top due to the lifting of unsaturated air. This effect, combined with evaporative cooling between the cloud and the dry air above, caused the initiation of a cool downdraft down the side of the cloud. A similar situation may be occurring over the Kauai mountains as unsaturated air above the inversion is forced up by the dynamical flow over the island combined with upward motion forced by deepening clouds. Strong evaporation at the inversion level, as the very moist air associated with the orographic cloud tops mixes with the drier air above, should cool the air above further. With the northeasterly trade flow this cool air should enhance the subsidence above lee slopes.

Why is Mount Waialeale one of the wettest spots on Earth?

This question is largely beyond the scope of this study; however some of the answer is present in these model results. The answer to the previous question explains

how 10 to 15 times more rainfall can fall over Waialeale than over the windward coast under trade wind conditions. Given the persistence of the trade winds the features described may explain a large fraction of the nearly 12,000 mm of rain recorded annually at the Waialeale rain gauge. Annually 1000 mm of rain occurs along the windward coast upwind therefore ten times that amount is 10,000 mm. The Kona low and shear line examples show that under less typical synoptic flow, rainfall is still persistent over W. During the winter time when trade winds are more frequently disrupted, the passage of fronts, shear lines, and kona systems provide Waialeale with high rainfall as well as other areas of the island.

The lower tropospheric structural changes that lead to large gradients in rainfall across the island are related to the following features of Kauai. The Hawaiian Islands lie in a consistent trade wind climate therefore the conditions that focus persistent rainfall (presence of TWI, moist layer top above the summit, moderate winds and associated orographic uplift, LCL below the mountain top) are present throughout large periods of the year. Other less frequent synoptic patterns will still tend to produce rain over Waialeale (as shown in the shear line and kona low cases) because 1) The flow of air off the ocean will consistently produce an LCL below the mountain summit; therefore uplift of air over Waialeale will aid cloud development and associated latent heating will aid flow over Waialeale. 2) Under periods of very weak winds, convergence of thermally driven (sea breeze) flows may tend to occur near the center of the island and along mountain ridges during the day. Showers generated may therefore occur over the mountains in the center of the island where Waialeale is located. 3) From most wind directions (with the exception perhaps of the NW) air reaches Waialeale without

encountering large mountains that consistently lie above the LCL; therefore upwind orographic rainfall is minimized. 4) The particular shape of the very steep east facing cirque of cliffs of Waialeale may tend to force strong ascending motion under conditions of wind with an easterly component. There may be a complex microclimate in this region of such dramatic topography (that is largely smoothed out from the 1 km grid) and large rainfall gradients. 5) Precipitation falling from an upper level cloud that falls through a cap cloud over Waialeale will produce larger rainfall droplets over Waialeale than over cloud free areas.

6.3 Future Work:

To assess the relative importance of different processes in producing rainfall over Kauai, it would be sensible to perform idealized case studies. These case studies could use a similar approach to Chen and Feng (2000) to establish the roles of processes such as latent heating and trade wind inversion height on the airflow over the island and the production of orographic rainfall.

The case studies here have stuck to a specific model setup. It would be useful to know how sensitive the results are to different model setups (cumulus scheme, PBL scheme, etc.). It would also be very important to assess which setup produces the best agreement with observations; this "tuning" step is often taken in optimizing forecast models.

More accurate landscape in the model should help improve the accuracy of the simulations. More accurate soil and vegetation data for the Hawaiian Islands should be incorporated into future simulations. Accurate soil and vegetation data is likely to be important for the accurate simulation of land surface energy budget and therefore for land

and sea breezes. The current setup has considerable smoothing of the mountain terrain with the maximum elevation being about 170 m below the actual highest point. 170 m of elevation difference may cause a big difference in the rainfall totals and distributions around Waialeale where there are such high rainfall gradients. Higher resolution terrain data, or the use of alternative elevation smoothing techniques (e.g. envelope topography), should help improve the realism of the model's mountains and valleys.

Theoretical islands with different shapes and peak elevations could be used to determine whether Kauai has the optimal shape for generating rainfall over the summit. Islands with 1600 – 2500 m peak elevations would be interesting tests because they would lie close to the inversion top and there are no real examples in the Hawaiian chain.

Case	Key points from simulation
Easterly wind	• The closest to typical trade wind conditions. • Fr ≈ 0.66 → strong orographic lifting. • Leeward dry intrusion of air, moist layer top "pulled" down by downward motion over lee slopes. • Moist layer deepens over windward Kauai • Upward to down motion transition triggers rainfall over W • Gradients in rainfall and rainfall totals agree well with observations • Large rainfall gradients linked to the proximity of the moist layer top to the mountain top
Weak southwesterly wind	• Weak winds, shallow moist layer • Fr ≈ 0.33 and stable → weak orographic lifting • Only shallow cloud development and very little rain, none over W. • Diurnal circulations develop
Shear line	• Goes through three stages: pre-shear line, shear line passage, and post-shear line. • Fr ≈ 0.66 • Deep moist layer during shear line passage produces widespread rain across the island • In contrast post-shear line shallower moist layer focuses rain over mountains, particularly W.

Strong northeasterly wind	• Model produces roughly 3 to 4 times more rainfall than observed. • Fr ≈ 1 ➔ strong vertical motion transition over W • Very large gradients in rainfall across the island, particularly down lee slopes
Kona low	• Weak winds but unstable air mass produce numerous convective rainfall events • Fr ≈ 0.33 • Convection is triggered over the island particularly over the mountains • East component of wind + daytime upslope flow may have helped trigger rainfall near W • Nocturnal convergence between land breeze and open ocean winds may have triggered vigorous convection and torrential showers over southern areas.

Table 3: Key summary points of simulations.

6.4 Conclusion:

This research has considered five three-day high-resolution case studies using the MM5 model focusing on the island of Kauai. Key results of the five cases are summarized in Table 3. Results from the easterly wind case study produced a realistic distribution of rainfall across the island, suggesting that the model correctly modeled the rainfall generation processes over the island under these conditions. Closer inspection of this case revealed that a number of structural changes were occurring to the moist trade wind layer as the moist air passed over the island. The size and shape of the island enabled air to flow over the mountains rather than splitting (blocked) around the sides for a period of trade wind orographic rainfall. Flow over the island lifted the top of the moist layer over the mountains, particularly over Waialeale. Upward moving air over windward areas triggered cloud development and deepening. Rainfall was heaviest over Waileale and was linked to the transition from upward motion over windward slopes to downward motion down lee slopes. The magnitude of this vertical motion transition is

likely to be strongly dependent on the height and structure of the trade wind inversion as well as the large scale wind speed and moist processes within the cloud. Previous studies suggest that the transition from upward moving air to downward moving air will trigger the fall out of large amounts of rain droplets, thus producing a rainfall maximum where the greatest volume of these droplets land. This occurs over Mt Waialeale according to both the model and observations (although a lack of an observational network in this area cannot confirm the exact location of the maximum).

Downward motion over lee slopes advected dry air from aloft with the moist layer below. This led to a drying, though also sometimes deepening, of the moist layer over lee areas of the island. Moisture was also removed from the layer through rainfall over windward and mountain areas although it is unclear how significant this effect is. General down-slope air motion coupled with a drier moist layer than upwind inhibits cloud development over lee areas and therefore rainfall.

Other case studies showed different rainfall amounts and distributions, but there was still a clear maximum over Waialeale for 4 out of the 5 cases. The exception was a period of light southwesterly winds and a shallow moist layer. Weaker orographic uplift due to weaker winds led to less deepening of the already shallow moist layer over the island. Thus orographic cloud development was inhibited and no significant rain fell at the summit.

Vegetation sensitivity case studies revealed that changing vegetation type over the island had an impact on the rainfall distribution. Changes to surface fluxes of momentum, heat, and moisture associated with vegetation change may be affecting the modeled rainfall distributions over the island. Alternatively the generation of different

cloud and rainfall systems associated with a separate simulation may be largely (if not entirely) responsible for the different rainfall distributions produced by the model. Further investigation is warranted on the role of vegetation on Hawaiian microclimates.

A modeled trade wind flow example over the island produces rainfall totals and gradients that agree with observations both for the simulation period and correlate with the annually observed pattern. The model produces significant small-scale structural changes to the trade wind layer over the island. These have been analyzed in this study to explain the rainfall distribution. Because of the dominance of trade winds in Hawaiian weather the structural changes described are hypothesized as the key to explaining why Mt Waialeale is one of the wettest spots on Earth.

7 Appendix:

I. THE WORLD'S WETTEST SPOT?

The estimated open ocean rainfall in the vicinity of the Hawaiian Islands is estimated at between 560 mm and 700 mm (Giambelluca and Schroeder, 1998). The average annual rainfall recorded at the Mt Waialeale rain gauge in central Kauai is 11,300 mm (Giambelluca and Schroeder, 1998). Other sources quote different values that likely correspond to different averaging periods such as 11,684 mm (NCDC), 13,000 mm (Suri 2002), and 11,531 mm (Nullet and McGranaghan, 1988). This annual average ranks as one of the largest in the world, competing with two stations in northeast India (Mawsynram, 11,871 mm (NCDC), and Cherrapunji, 10,820 mm (Suri 2002)) and a couple of locations in Columbia (Lloro, 13,300 mm (estimate NCDC) and Mt Tutenendo, 11,770-12,045 mm (Suri 2002)) that all apparently have totals within the same ball park. It is not clear which of these locations actually has the largest average annual rainfall total as it depends on the sampling periods and on measurement practices (NCDC). There may be locations near these stations or in totally different locations that receive more annual rainfall. It is unlikely that any of these rain gauges have been placed exactly at the wettest spot. It is also unlikely (impossible) that any of the rain gauges are measuring precisely the actual rainfall totals that fall over these locations because of errors associated with rainfall measurement. Improving numerical models may help identify other remote locations that may receive similar or larger annual totals. For example Rozell (1999) states that a location in the coastal mountains of Alaska was modeled to produce a similar annual total to the stations mentioned above if one included

the snow equivalent rainfall. These findings from models will have to be observationally verified for them to have any weight.

Finally yet another contender lies on the windward slopes of the Piton de la Fournaise massif on Reunion Island, east of Madagascar. Already the holder of a number of shorter period rainfall records, associated with orographic enhancement of tropical cyclone rainfall, Reunion Island also appears to have areas that compete for the largest annual rainfall on Earth. A rain gauge station at 1600 m, called Baril 1600, was set up in 1993 and in its first (apparently not exceptionally wet) year recorded 18,000 mm (Barcelo and Coudray 1996). Subsequent totals from this station and others have led Barcelo and Coudray to define an area over the windward slopes as having over 12,000 mm of annual rainfall. If this is correct then this area may have more rain than the area around the Waialeale rain gauge.

Regardless of these uncertainties we can safely say that Mount Waialeale is one of the contenders for the title of 'world's wettest spot'. It may also be the location with the most days in a year where measurable rain falls. On an estimated 335-360 days in a year rain falls at the Waialeale rain gauge. This is likely to be much greater than the number of rain days at the stations in NE India given that their rainfall is strongly dependent on the seasons with the vast majority of the rainfall falling in the summer. I am uncertain about the number of rainy days at the Columbian stations.

8 References:

Anthes, R. A., 1984: Enhancement of convective precipitation by mesoscale variations in vegetative covering in semi-arid regions. *J. Clim. Appl. Met.*, **23**, 541-554.

Anthes, R. A., and T. T. Warner, 1978: Development of hydrodynamical model suitable for air pollution and other mesometeorological studies. *Mon. Wea. Rev.*, **106,** 1045-1078.

Barcelo, A. and J. Coudray, 1996: (Summary of) New annual isohyet and rainfall maximum map for the Piton de la Fournaise (Reunion Island). *Rev. Sci. Eau* 9 (4): 435-455 [article in French]. http://www.rse.uquebec.ca/ang/vol19/v9n4a3.htm

Blythe, E. M., A. J. Dolman, and J. Noilan, 1994: The effect of forest on mesoscale rainfall: an example from HAPEX-MOBILHY, *J. Appl. Met.* **33,** 445-454.

Businger, S., T. Birchard, K. Kodama, P. A. Jendrowski, and J-J. Wang, 1998: A bow echo and severe weather associated with a kona low in Hawaii. *Wea. and Forecasting*, **13**, 576-591.

Chen, Y-L., and J. Feng, 2001: Numerical simulations of airflow and cloud distributions over the windward side of the island of Hawaii. Part 1: The effects of trade wind inversion. *Mon. Wea. Rev.*, **129**, 1117-1133.

Chen, Y-L., and J-J. Wang, 1994: Diurnal variation of surface thermodynamic fields on the island of Hawaii, *Mon. Wea. Rev.*, **122**, 2125-2138.

Chen, F., T. T. Warner, and K. Manning, 2001: Sensitivity of orographic moist convection to landscape variability: A study of the Buffalo Creek, Colorado, flash flood case of 1996, *J. Atmos. Sci*, **58**, 3204-3223.

Dudhia, J., 1993: A nonhydrostatic version of the Penn State-NCAR mesoscale model:

validation tests and simulation of an Atlantic cyclone and cold front. *Mon. Wea. Rev.* **121,** 1493-1513.

Durran, D., 1986: Another look at down slope windstorms. Part 1: The developments of analogs to supercritical flow in an infinitely deep, continuously stratified layer. *J. Atmos. Sci.* **43,** No. 21, 2527-2543.

George, J. J., 1960: Weather forecasting for aeronautics. *Academic Press.* 673 pp (see pp 411-415)

Giambelluca, T. W., and T. A. Schroeder, 1998: Climate. *Atlas of Hawaii (Juvik, S. P., and Juvik, J. O. (Eds.))*, 49-59.

Giambelluca, T. W., M. A. Nullet, T. A. Schroeder, 1986: Rainfall atlas of Hawaii. Rep. R 76, State of Hawaii, Dept. of Land and Natural Resources, 267 pp.

Grell, G. A., 1993: Prognostic evaluation of assumptions used by cumulus parameterizations. *Mon. Wea. Rev.*, **121**, 764-787.

Hall, W. D., 1980: A detailed microphysical model within a two-dimensional framework: model description and preliminary results. *J. Atmos. Sci.*, **37,** 2486-2507.

Hong, S-Y., H-L Pan, 1996: Nonlocal boundary layer vertical diffusion in a medium range model. *Mon. Wea. Rev.*, **124,** 2322-2338.

Lavoie, R. L., 1974: A numerical model of trade wind weather on Oahu. *Mon. Wea. Rev.*, **102,** 630-637.

Leopold, L. B., 1949: The interaction of trade wind and sea breeze, Hawaii. *J. Meteor.*, **6,** 312-320.

Lyons, S. W., 1982: Empirical orthogonal function analysis of Hawaiian rainfall. *J. Appl. Met.*, **21,** 1713-1729.

MMM/NCAR, 2000: PSU/NCAR mesoscale modeling system tutorial class notes and user's guide: MM5 modeling system version 3. *Mesoscale and Microscale Meteorology Division National Center for Atmospheric Research.*

NCDC (National Climate Data Center), http://www.ncdc.noaa.gov/oa/climate/globalextremes.html

Nobre, C. A., P. J. Sellers, and J. Shukla, 1991: Amazonian Deforestation and Regional Climate Change, *J. Clim.*, **4,** 957-988.

Nullet, D., and M. Mcgranaghan, 1998: Rainfall enhancement over the Hawaiian Islands. *J. Clim.*, **Vol. 1 No. 8,** 837-840.

Ramage, C. S., and T. A. Schroeder, 1999: Trade wind rainfall atop Mount Waialeale, Kauai. *Mon. Wea. Rev.*, **127,** 2217-2226.

Reap, R. M., and D. S. Foster, 1979: Automated 12-36 hour probability forecasts of thunderstorms and severe local storms. *J. App. Met.* **18,** 1304-1315.

Reisner, J., R. M. Rasmussen, and R. T. Bruintjes, 1998: Explicit forecasting of supercooled liquid water in winter storms using the MM5 mesoscale model. *Q. J. R. Met. Soc.*, **124,** 1071-1107.

Rozel, N., 1999: Alaska has the highest, the coldest, the wettest? Article #1440 *Alaska Science Forum,* http://www.gi.alaska.edu/ScienceForum/ASF14/1440.html

Sanderson, M., Ed., 1993. *Prevailing Trade Winds, Weather and Climate in Hawaii.* University of Hawaii Press, 126pp.

Smolarkiewicz, P. K., R. M. Rasmussen, and T. L. Clark, 1988: On the dynamics of Hawaiian cloud bands: island forcing. *J. Atmos. Sci.*, **45,** 1872-1904

Smorlarkiewicz, P. K., and R. M. Rasmussen, 1989: Low Froude number flow past three-

dimensional obstacles. Part I: Baroclinically generated lee vortices. *J. Atmos. Sci.*, **46,** 1154-1164.

Sud, Y. C., G. K. Walker, J-H. Kim, G. E. Liston, P. J. Sellers, and W. K-M. Lau, 1996: Biophysical consequences of a tropical deforestation scenario: a GCM simulation study, *J. Clim.* **9,** 3225-3247.

Suri, D., 2002: So where is the wettest place in the world then?, http://www.dandantheweatherman.com/Pikanto/wettestplace.html

References taken from:

Ahrens, C.D. (2000): *Meteorology Today*, Brooks/Cole, p.528.

Bodin, S. (1978): *Weather and Climate*, Blandford, p.272.

Holford, I. (1977): *The Guiness Book of Weather Records*, Book Club Associates, p.240.

Kroll, E. (1995): *De Wereld van het Weer*, Teleac, p.188.

Raikhel, E. (2000): Extreme Weather. *Scientific American Presents*, 11, 40-41.

Simons, P. (1996): *Wierd Weather*, Little Brown and Company, p.303.

Takahashi, T., 1981: Warm rain study in Hawaii – Rain initiation. *J. Atmos. Sci.*, **38,** 347-369.

Wang, J-J., H-M. H. Juang, K. Kodama, S. Businger, Y-L Chen, and J. Partain, 1998: Application fo the NCEP Regional Spectral Model to improve mesoscale weather forecasts in Hawaii. *Wea. Forecasting,* **13**, 290-305.

Woodcock, A. H., 1975: Anomalous orographic rains of Hawaii. *Mon. Wea. Rev.*, **103,** 334-343.